

ISSN : 0025-0422

JOURNAL  
OF  
THE MAHARAJA SAYAJIRAO UNIVERSITY OF BARODA



सत्यं शिवं सुन्दरम्  
Estd. 1949

Accredited Grade 'A' by NAAC

VOL. 54 NO. 1 (Science & Technology)  
Vadodara  
2020



**JOURNAL  
OF  
THE MAHARAJA SAYAJIRAO UNIVERSITY OF BARODA**

Vice-Chancellor  
Parimal Vyas

Pro-Vice-Chancellor  
Vacant

**Editorial Board**

C. N. Murthy  
(Editor)

A. C. Sharma  
(Physical Sciences)

Arun Pratap  
(Physical Sciences)

A. V. Bedekar  
(Chemical Sciences)

H. M. Patel  
(Engineering Sciences)

K. Muralidharan  
(Mathematical Sciences)

L. S. Chamyal  
(Environmental & Geological Sciences)

Rasheedunnissa Begum  
(Biological & Pharmaceutical Sciences)

JOURNAL  
OF  
THE MAHARAJA SAYAJIRAO  
UNIVERSITY OF BARODA

EDITOR  
Prof. C. N. MURTHY



सत्यं शिवं सुन्दरम्  
Estd. 1949

**Accredited Grade 'A' by NAAC**

VOL. 54 NO. 1  
(SCIENCE & TECHNOLOGY)  
VADODARA  
2020

ISSN : 0025-0422

---

Printed by **Shri Jatin H. Somani**, Manager, The Maharaja Sayajirao University of Baroda Press (Sadhana Press), Near Palace Gate, Palace Road, Vadodara, and Edited by **Prof. C. N. Murthy**, Editor (Science & Technology) at the Maharaja Sayajirao University of Baroda, Vadodara - 390 002, (India), February 2021.

## CONTENTS

Sr. No.	Topic	Page No.
1.	SEVERLESS ARCHITECTURE FOR BIG DATA PROCESSING IN ENTERPRISE DATA HUB A. Murugan, S. Ganesan	1-14
2.	USEFULNESS OF REMOTE-SENSING AND GIS TECHNIQUES IN ESTIMATING SURFACE VELOCITY, ICE-THICKNESS AND VOLUME OF GLACIER C. U. Dongare, B. S. Deota	15-27
3.	A BAYESIAN APPROACH TO THE OPTIMAL WARRANTY LENGTH FOR PARETO DISTRIBUTED PRODUCT WITH MULTIPLY TYPE-II CENSORING SCHEME D. T. Patel, M. N. Patel	29-54
4.	NON-LINEAR FINITE ELEMENT ANALYSIS OF STRESS AND STRESS INTENSITY FACTOR ACROSS THE ADHESIVE THICKNESS IN COMPOSITE SINGLE-LAP JOINTS J. D. Rathod, K. Sheth	55-70
5.	ANALYSIS OF EARLIEST DEADLINE FORST AND RATE MONOTONIC SCHEDULING ALGORITHM IN SOFT REAL-TIME SYSTEM J. Teraiya, A. Shah	71-80
6.	FINET : FACIAL EXPRESSION RECOGNITION BASED ON FUSION INHERITED NETWORK V. Mokaya, M. Gupta, M. Bansal	81-93

# SERVERLESS ARCHITECTURE FOR BIG DATA PROCESSING IN ENTERPRISE DATA HUB

**A. Murugan, S. Ganesan**

PG & Research Dept. of Computer Science, Dr. Ambedkar Govt. Arts College,  
University of Madras, Chennai, India  
E-mail : amurugan1972@gmail.com

## **Abstract**

In the era of modern utility computing theory, Serverless architecture is the cloud platform concept to hide the server usage from the development community and runs the code on-demand basis. Key objective is to abstract the infrastructure complexities of server management and scaling, but metered payment for processed requests only. This paper provides an algorithm to handle enterprise data hub using efficient serverless architecture for the complex big data query processing. This paper depicts about the experimental advantage of execution time optimization with agile availability and cost reduction of the underlying infrastructure, using new design of Serverless architecture.

**Keyword:** Serverless, Utility computing, Big Data, Scaling, Metered payment, Enterprise Data Hub, etc.

## **1. Introduction**

Data is foundation of the computer industry. In the rapid transformation of Information Technology, enterprise data growth is phenomenal. Enterprise Data Hub (EDH) is a solution to build and maintain the golden records of any enterprise as shared trustable enterprise data. With the big data Map Reduce algorithm, EDH is easily built using the traditional computing model. In recent industry days, serverless computing is highly adopted due to favorable small, self-contained units of computation, which makes the big data process easier to manage and scale in the cloud. Serverless computing programming model is highly influenced with inherit model of non-maintenance state of the underlying application. This paper depicts about the efficient way of utility computing to handle the data in the most effective logic. Key logic of this paper, is to build the serverless computing for EDH design.

## 2. Literature Review

### A. Enterprise Data Hub

Enterprise Data Hub is a solution to build and maintain the golden records of any enterprise as shared trustable enterprise data. It is the proposed solution which is a central data repository for any enterprise with open sourced Big Data tools and techniques like HCatalog (Reference Data), Data Wrangler (cleansing), Hadoop Distribution File System, Map Reduce, Hive (distributed process). The final output of this framework is Master data.

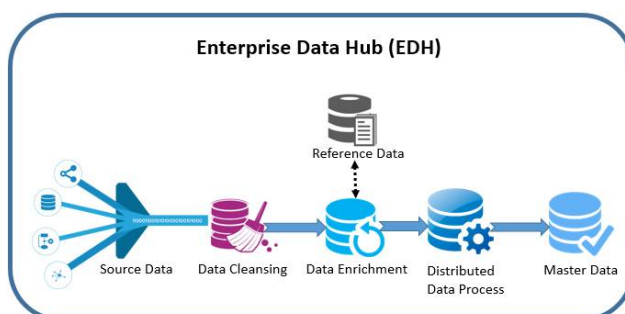


**Figure 1. Reference Architecture of EDH**

### B. Shift in Serverless Architecture

The word 'Serverless' doesn't literally mean as 'no server'. It leads to emerge Function as a Service (FaaS) concept. It allows small pieces of code represented as functions to run for limited amount of time on demand basis in the cloud.

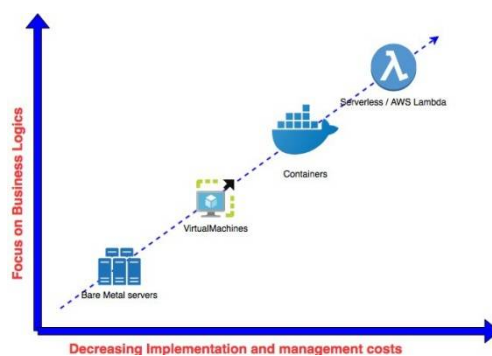


**Figure 2. Architecture Evolution of Serverless Computing**

As depicted above, the physical machines took months to deploy any system in production with the life cycle in years. On evolution of VM and containers concepts, serverless computation deploy the production ready code with self-contained small units in the cloud.

### 3. Serverless Architecture

#### A. Definition

Serverless Architecture is disruptive design pattern to support the modern utility computing. It incorporates the custom written code along with third party services, in managed and ephemeral containers. This concept is terms as “Functions as a Service” (FaaS) platform. In a nutshell, FaaS executes the backend code with own short lived server application and defined as Serverless Architecture.

The ephemeral and stateless nature of the serverless micro services and functions that make up the modern distributed application is great for agility and scalability.

#### B. Industry Use Case

Allied Market Research report estimated the global serverless architecture market was worth ~\$3.1 billion in 2017, and forecasts to ~\$22 billion by 2025 with annual growth rate of 28%

Here is an industry use case to implement serverless architecture in an online shopping store.

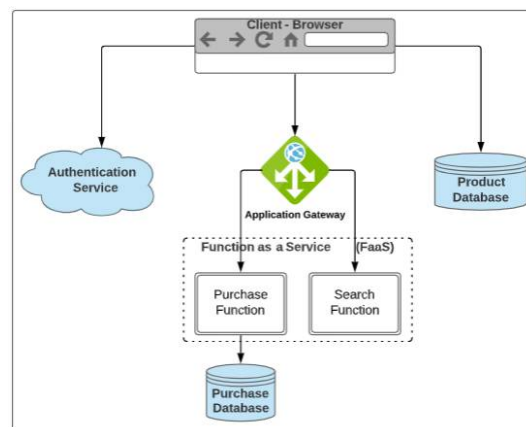


**Figure 3. Online shopping store**

This design helps to parallelize into independent units of work in asynchronous and concurrent mode without worrying about the underlying infrastructure. In

terms of changing business requirements, it is highly dynamic for accelerated developer velocity.

### C. Message Driven Design - Illustration

Message driven design is the best suit for the serverless computing. In theory of computer architecture, message driven design is built based on the asynchronous communication. A message is a simple data transfer object (DTO) with message name and details. On arrival/dispatch of any message, the system triggers a function to execute. It is the fundamental of message driven application.

The context is usage of message driven design in FaaS. Let us consider a real life application – Advertisement (Ad) server. Traditionally, Ad Server is designed synchronously with the response to the user click operation in a channel. In terms of operation, the user clicks on the advertisement content in the browser and the server collects the relevant information for further processing.

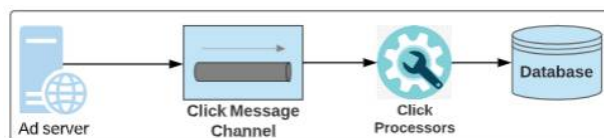


**Figure 4. FaaS Message Driven Design**

As illustrated in the above design, it is redesigned with message consumer model using FaaS function of asynchronous message processing is a very popular use case for serverless architecture. This function runs within the event-driven context the vendor provides. FaaS is distinct to process several messages in parallel by instantiating multiple copies of the function code. Programmer doesn't need to worry about the underlying infrastructure as it is taken care by serverless technologies.

### D. Benefits of Serverless computing

**Scalability:** Cloud's scalability is one of the powerful automatic mechanism to increase the infrastructure capacity dynamically. As serverless technologies handle the scaling demand seamlessly, software developers don't have to worry about the infrastructure policies.

**Simplified server execution:** FaaS is the core design of the serverless computing. It perform the single purpose function independently like general API call by abstracting the execution complexity.

Serverless architecture for big data processing in enterprise data hub

**Time to Market:** Serverless architecture makes the availability of the program instantly and so it significantly reduces the software deployment cycle. As the result, the software launching time to market is quite fast.

**Cost advantage:** Traditional computing needs an upfront capital cost to purchase the physical servers well in advance. Serverless computing requires only the operational cost, no upfront capital. The rate of cost advantage is depicted as below for the serverless computing.

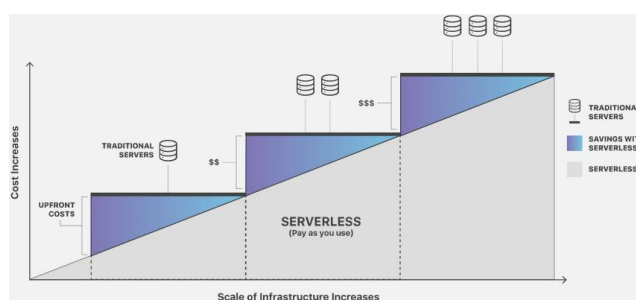


**Figure 5. Cost Advantage of Serverless Computing**

#### *E. Limitation of Serverless computing*

No long term task: By design, serverless computing is intentionally ephemeral. As the execution is sustained for few minutes in the cloud, it doesn't fit for long running tasks. Also, it doesn't retain any stateful data of the previous run.

## **4. Technical Implementation**

### *A. Top-k Pricing algorithm using Map Reduce*

Map Reduce is an algorithm to process and generate big data result with parallel and distributed computing concepts. Its implementation consists of a:

1. Map function that performs filtering and sorting of the given big data set, and a
2. Reduce function that performs a summary operation on the output of the Map function

Top-k share pricing search is one of the key functionalities in Enterprise Data Hub. Source data is ingested from New York Stock Exchange web site into Hadoop file system. Perceived historical data is queried by the user with Top-k stock details based on its closing price.

Pseudo code is drafted with parallel top-k query processing using Google's Map Reduce programming model.

Mapper processes the key value pair at a time and writes them as intermediate output on local disk. To do that, whole block is processed with key value pairs to find top-k result.

---

Algorithm: Map algorithm to process the big data

Input: Raw data to be processed

Output: Intermediate output on local disk

---

***begin***

*Get the input of Object as key*

*Get the input of Text as value*

*Get the input of Context as context*

***function Type[] map***

***begin***

*Let tokens = value.split("\t");*

*Let price = tokens[0];*

*Let topPrice = parse (tokens[1]);*

*Let topPrice = (-1) \* topPrice;*

*Write context as topPrice, price;*

***end***

***end***

Reducer processes the key value pair at a time and writes them as final output on Hadoop Distributed File System. Pseudo code of Reducer function is depicted here.

Algorithm: Reduce algorithm to produce the final data

Input: Intermediate output on local disk

Output: Final processed big data result

***begin***

*Get the input of LongWritable as key*

*Get the input of Iterable Text as value*

*Get the input of Context as context*

***function Type[] reduce***

***begin***

*Let price = null;*

*Let topPrice = (-1) \* key.get();*

*for each (Text val in values)*

*begin*

*Let price = val;*

*end*

*if (count < k)*

*begin*

*Write the context as topPrice;*

*count ++;*

*end*

*end*

*end*

In the above map reduce algorithm, it is evident to implement the efficient process of all key value pairs with lot of data movement in asynchronous functions.

### B. Serverless FaaS Design

Function-as-a-Service (FaaS) is the core design of serverless computing. It consists of smaller functions, which are managed by the cloud provided infrastructure. This new architecture model helps the various application patters like event handler, invocation patterns and compute-intensive big data process.

The abstraction level of FaaS architecture is depicted as below. It contains front end layer named Edge and back end layer named Master. On receipt of the various front end hits, Event Queue orchestrates the incoming request to Dispatcher component. By design, FaaS has multiple instances of the smaller functions as Worker. Dispatcher maintains and routes the job request to the distributed worker list in the Master layer.

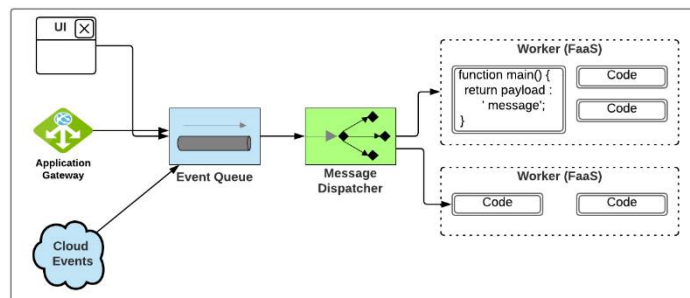


**Figure 6. Serverless FaaS Architecture**

Typically, FaaS programming model consists of two major primitives namely Action and Trigger.

1. **Action:** Stateless function to execute arbitrary code.
2. **Trigger:** Events class from a variety of sources.

Actions can be invoked asynchronously either via REST API or based on trigger. A single event can trigger the multiple functions for parallel invocations. In contrast, the result of an action can trigger another function as sequential invocations.

```
function main (params, context)  
begin  
  return { payload:  
    'stock name ' + params.name +  
    'top price ' +params.price  
  }  
end
```

In the above serverless code, main function takes a dictionary using JSON object as input and produces output in dictionary format. By design, serverless functions don't maintain the state between the executions. So, the program has to handle to retrieve and update any needed state with context object.

### *C. Serverless FaaS based Top-k algorithm*

This serverless FaaS based map reduce top-k algorithm has three key components namely

1. load processor
2. mapper
3. reducer

Initially, stock price data files is stored in the landing folder. It triggers the first task named load processor, which picks up the data file to process and load into mapper function of the algorithm. Mapper processes the input data to produce key value pairs. Reducer picks up the output of the Mapper to aggregate and produce the desired results.

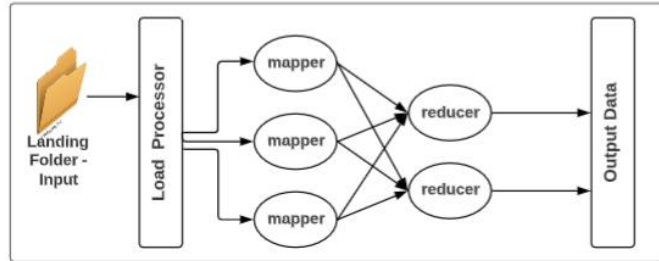


**Figure 7. Serverless Map Reduce Components**

Mapper function splits the input of load processor into key/value pairs to proceed further. Mathematically, the size of the data chunk to be processed by each mapper is:

$$\text{chunk size} = \frac{\text{total data size}}{N_{mappers}}$$

where dividend is total data size of the input content and divisor is number of Mapper function.

Prior to pass the input from load processor to mapper function, it verifies 'chunk size' to satisfy the below conditions:

[1] If chunk size is smaller than the minimum block size specified by the user, chunk size will be set to Min block size. By doing so, the number of mapper function is calculated as:

$$N_{mappers} = \text{int} \left( \frac{\text{total data size}}{\text{Min block size}} \right) + 1$$

[2] If chunk size is higher than the calculated safe memory size of the underlying system, then safe memory size is calculated as a percentage of the memory assigned to the mapper functions. To fit the data in mapper function, the number of mapper function is calculated as:

$$N_{mappers} = \text{int} \left( \frac{\text{total data size}}{\text{Safe memory size}} \right) + 1$$

[3] In case of chunk size is higher than the maximum block size, it will be set to Max block size, which leads to calculate the number of mapper function as:

$$N_{mappers} = \text{int} \left( \frac{\text{total data size}}{\text{Max block size}} \right) + 1$$

The algorithm covered the possible conditions to recalculate the number of mappers function. In all scenarios, the load processor always adds one extra mapper with the responsibility to process the residual data chunk. The size of the residual data is calculated as:

$$\text{residual data} = \text{total data size} - (N_{mappers} - 1) * \text{chunk size}$$

This approach prevents any mapper to process its corresponding chunk plus the mentioned residual data, what could cause an additional overload in that mapper. It is efficient to distribute the load across multiple reducers if the keys are not well distributed in the input data. To do so, it is vital to hash the keys using numbers and extract the residual part of the integer division with the total number of reducers. Mathematically, it was represented as:

$$\text{reducer size} = \text{hash}(\text{key}) \% N_{reduce}$$

Thus, map reduce algorithm is extended with serverless architecture for processing top-k pricing data.

## 5. Experimentation Result

### F. System Environment

To evaluate the proposed serverless algorithm, 5 nodes of virtual Linux servers are created in Amazon cloud environment. Sample data volume of 90 million rows with 6.39 GB sized content. Python 2.7 and Node.js software are used to develop the program. The system uses Amazon cloud's Lambda in conjunction with Amazon S3 to build a Map Reduce framework that can process data stored in S3.

Amazon Lambda provides the cloud platform for the execution of high throughput job. Each serverless Lambda function provides the service of memory between 128 to 3,008 MB, disk storage of 75 GB, concurrent execution of 1,000 tasks and timeout of 15 minutes.

### B. Execution Time Optimization

Serverless big data map reduce top-k algorithm is benchmarked to measure the response time with meaningful queries – scan & aggregation. The function is executed against disk based algorithms – Hive & Serverless map reduce with three handful use cases.

**Table 1. Experimented Result – Data Retrieval Time**

Disk based Algorithms	Execution (in seconds)		
	Scan-1000	Scan-100	Aggregation
Hive	52.4	61.5	741.1
Serverless map reduce	38.3	48.2	202

The execution data set contains 90 million rows and approximately 636 GB of data volume. Scan queries are built to select Top-k price value where  $k > z$ , with the constraint of  $z = \{1000, 100\}$ . The two scan queries are tested and execution time is captured against disk based hive and serverless map reduce algorithms.

Aggregation is the most complex query in any database management system. Serverless map reduce algorithm is more efficient than hive execution time. The data set 775 million rows with approximately 127GB disk size. The aggregate query covers the pricing field in Group By condition.

Experimented execution results are marked in the above table to demonstrate the time efficiency. Data points are graphically represented as below.

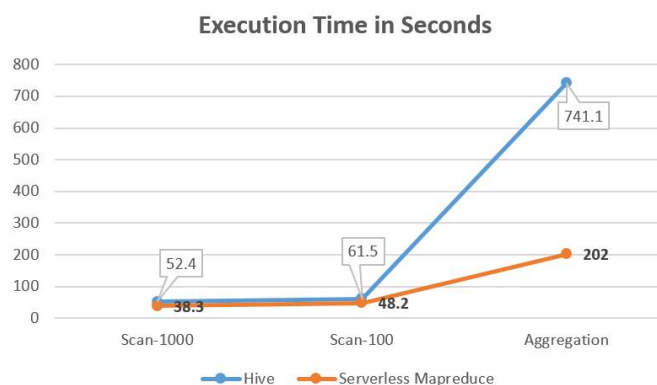


**Figure 8. Comparison chart of Scan & Aggregation queries**

Result shows the huge improvement of big data retrieval execution time between hive and serverless map reduce algorithms. When the rate of data volume and complexity of queries increase, the execution time efficiency is improved as shown in the experimented result graph.

### Conclusions

This paper describes an improved version of big data map reduce algorithm, by leveraging the emerging serverless architecture. Amazon Lambda framework is used to implement serverless architecture in this paper. The core logic is to invoke Function as a Service in response to the distributed data based on the number of simultaneous mapper function. On comparing the performance of serverless architecture against Hive, it has an impact on the execution time efficiency of big data map reduce queries.

This research paper concludes the technical strength of new serverless architecture, using the experimental results on big data queries. Thus, enterprise data hub can leverage the state of the most efficient architecture to execute the big data processing Top-k algorithm.

### References

- [1] Ganesan S. and Murugan A., "Top-k Equities Pricing Search in the Large Historical data set of NYSE", International Journal of Computational Intelligence Research, Volume 13 Number 1 pp 161-173, 2017
- [2] Bernstein D., "Containers and cloud: From LXC to Docker to Kubernetes", IEEE Cloud Computing 1, 3 (Sept. 2014), 8184
- [3] Baldini I., "Serverless computing: Current trends and open problems", Research Advances in Cloud Computing, Springer, 2017, 120
- [4] CNCF Serverless White Paper, <https://github.com/cncf/wg-serverless>, whitepaper
- [5] Yan M., Castro P., Cheng P. and Ishakian V., "Building a chatbot with serverless computing", In Proceedings of the 1st Intern Workshop on Mashups of Things, 2016
- [6] Ye W., Khan A.I. and Kendall E.A., "Distributed network file storage for a serverless (P2P) network", In Proceedings of the 11th IEEE Intern. Conf. on Networks, 2003, 343347
- [7] Wang L., Li M., Zhang Y., Ristenpart T. and Swift M., "Peeking behind the curtains of serverless platforms", In Proceedings of USENIX Annual Technical Conf., 2018, 133146. USENIX Association

- [8] Lin W-T, Krintz C., Wolski R., Zhang M., Cai X., Li T. and Xu W., “Tracking causal order in AWS lambda applications”, In Proceedings of the IEEE Intern. Conf. on Cloud Engineering, 2018
- [9] Baldini I., Castro P., Cheng P., Fink S., Ishakian V., Mitchell N., Muthusamy V., Rabbah R., Suter P., “Cloud-native, event-based programming for mobile applications”, In Proceedings of the Intern. Conf. on Mobile Software Engineering and Systems, 2016, 287288. ACM, New York, NY.
- [10] Etzioni O. and Niblett P., “Event Processing in Action”, Manning Publications Co., Greenwich, CT, 2010
- [11] Kilcioglu C. Rao, J.M. Kannan and McAfee R.P., “Usage patterns and the economics of the public cloud”, In Proceedings of the 26th Intern. Conf. World Wide Web, 2017
- [12] Oakes E., Yang L., Houck K., Harter T., Arpaci-Dusseau A.C. and Arpaci-Dusseau R.H., “Pipsqueak: Lean Lambdas with large libraries”, In Proceedings of 2017 IEEE 37th Intern. Conf. on Distributed Computing Systems Workshops, 395400
- [13] Lee H., Satyam K. and Fox G.C., “Evaluation of production serverless computing environments”, In Proceedings of IEEE Cloud Conf. Workshop on Serverless Computing (San Francisco, CA, 2018)

-----

# USEFULNESS OF REMOTE-SENSING AND GIS TECHNIQUES IN ESTIMATING SURFACE VELOCITY, ICE-THICKNESS AND VOLUME OF GLACIER

**C. U. Dongare, B. S. Deota**

Department of Geology, Faculty of Science, The Maharaja Sayajirao University of Baroda,  
Vadodara, Gujarat 390002, India.  
Email: chinmayd.avs@gmail.com

## **Abstract**

The present study emphasizes the techniques of remote sensing and GIS in the estimation of surface velocity, ice thickness and volume for a Himalayan glacier. Surface velocities over Janapa-Garang glacier were estimated by performing sub-pixel correlation of Landsat-8 L1TP imagery. Surface velocity varies within the glacier and ranges from 0.05 m/yr ~ 28 m/yr. Higher velocities occur in the inner portions of the glacier and lower velocities adjacent to the glacier boundaries. Ice-thickness is derived using laminar flow equation, parameterization scheme (slope dependent approach) and depth-area scaling method. The volume of the glacier is estimated using three existing volume-area scaling relations. The results of thickness and volume are found to match well with the existing glacier inventory of GSI 1999.

**Keywords:** Remote sensing & GIS, COSI-Corr, Surface Glacier Velocity, Ice thickness and glacier volume

## **1. Introduction**

Surface glacier velocity, ice-thickness and volume are the significant parameters useful in characterizing the dynamic behaviour and assessing the health of the glacier [1]. Long term estimations of the velocity can help in quantifying the mass balance of the glacier; it can also document us the state of the glacier and its response towards the fluctuations in climate [2-3]. Estimates of ice-thickness and volume are of greater interest from environmental (future sea-level rise, etc.) and socio-economic point of view (hydro-power generation, etc.) [4]. In-situ measurement of these parameters is often difficult for remotely situated glaciers. Rough terrain and inclement weather conditions limit the field studies. However, remote sensing techniques, because of their ingrained calibre of providing a synoptic view, timely data collection and repetitive coverage can serve as a potent and systematic medium to study glaciers situated in remote, inaccessible and

frosty environments [5]. Field studies for measuring surface velocity involves the installation of stakes in the glacier ice and monitoring their position with help of DGPS or total station. However, due to frequent loss of stakes and difficulty observed in carrying the measuring instruments to the site, data obtained is not sufficient to draw interpretation regarding the dynamic behaviour of the glacier [6]. Remote sensing techniques used for estimating surface glacier velocity are SAR interferometry, SAR image data intensity tracking techniques on satellite data or by applying sub-pixel correlation technique on the optical data. Literature suggests that optical image-based correlation techniques are more successful and robust compared to SAR based methods for mountain glaciers. In past, velocity data were estimated for Gangotri glacier [1], Chhota-Shigri glacier [6], PRG glacier [7] using optical image-based correlation technique and the results were in harmony with the field measurements. Field techniques available for ice-thickness and volume measurement are boreholes, ground-penetrating radar and radio-echo sounding, which are expensive, arduous to perform in difficult locations of the glaciers [4]. Alternatively, glacier thickness and volume estimates have been made based on the principles of ice flow [8-10]. Also, volume-area scaling relationships are widely accepted to estimate the glacier volume [11-13]. Here an attempt has been made to work on surface velocity, ice thickness and volume of Janapa-Garang glacier ( $31^{\circ}14'21''$  N Lat. to  $31^{\circ} 19' 16''$  N; Long.  $78^{\circ}23'51''$  E to  $78^{\circ}29'25''$  E) located in Baspa basin, Himachal Pradesh (Figure 1). For ease the glacier is represented in two parts as glacier-1 and glacier-2 in the current study (Figure 2). Surface velocities are estimated using remote sensing techniques [14]. Ice-thickness is derived using laminar flow equation [10], parameterization scheme [9] and depth-area scaling method [15]. While, the volume of the glacier is estimated using three existing volume-area scaling relations [13], [16-17].

## 2. Dataset

Cloud free Landsat 8 data of September month is used to get maximum exposure of the glacier (<http://earthexplorer.usgs.gov>) (Table 1). Landsat 8 data comprises of 11 bands of which particularly Band 8 (15 m Pan, wavelength 0.503-0.676) is used for velocity estimation.

## 3. Methods

(a) Calculation of Surface Velocity:

For calculation of surface velocity sub-pixel correlation of the acquired Landsat 8 images is carried out using open source software named COSI-Corr (Co-registration of Optically Sensed Image and correlation) [14]; freely downloadable from <http://www.tectonics.caltech.edu/>. Details about the algorithm are provided by Leprince et al. 2007. The algorithm performs the iterative cross-correlation of two images to find out the best possible correlation within them. The two images can be addressed as Pre-event and Post-event image. Sub-pixel correlation of these images is carried out by taking a sliding window of 128 x 8 pixels and a step size of 4 pixels. Working of COSI-Corr is shown in (Figure 3). As a result, three output images are obtained i.e. (i) E-W displacement image (ii) N-S displacement image (iii) SNR image which shows us the quality of the correlation or the accuracy of the correlation. The minimum threshold set is 0.9, which means that the pixels with less than 0.9 SNR are to be eliminated. Later the vector field is generated with the help of the E-W and N-S files and it is then overlaid on the image to ensure the general flow direction of the glacier. Once the alignment of the vectors is done properly the Euclidian distance formula expressed as equation (1) is applied to obtain the translational movement in Arc GIS 10.3 using the raster calculator tool. The AOI is then clipped using the clipping tool and finally, velocity (Figure 5) is calculated simply by dividing the movement by the time interval between the two scenes.

$$D = \sqrt{(E-N)^2 + (W-S)^2} \quad (1)$$

(b) Ice-thickness estimation:

Ice thickness is estimated using laminar flow equation [10] which is as follows:

$$u_s - u_b = \tau_b n (H)^{n+1} \quad (2)$$

The basic idea of the model for thickness estimation follows the logic of basal shear stress and velocities in the laminar flow. The glacier model (Figure 4) considered here is a parallel-sided slab of the ice having density  $\rho$  with the thickness  $H$  occurring on the rough plane having the slope  $\alpha$ . The assumption made here is that the slab does not slide on the plane and secondly the thickness of the slab is less than its length and width. The slab is perpendicular to the plane and has unit cross-section; the weight of the slab is  $\rho g H$ . This weight of the slab is balanced by the basal shear stress  $\tau_b$ . This is expressed mathematically as equation (3):

$$\tau_b = \rho g H \sin \alpha \quad (3)$$

From equation (2) and (3) we have,

$$H = (4)$$

Where,  $u_s$  = Surface velocity;  $u_b$  = Basal Velocity;  $u_b = 0.25u_s$  [18];  $n$  = Glen's flow law exponent ( $n=3$ );  $A$  = Creep Parameter having value of  $3.24 \times 10^{-24} \text{ Pa}^{-3} \text{ s}^{-1}$  for temperate glacier [10],  $f = 0.8$  [9],  $\rho = 900 \text{ kg/m}^3$  [8],  $g$  is gravitational acceleration  $9.8 \text{ m/s}^2$ . Six points were selected on each glacier along the central flow line. The point velocity and slope for those points were obtained in Arc GIS 10.3 and were substituted in the equation (4). The results were averaged out to obtain the mean ice-thickness for Janapa-Garang glacier.

To quantify the uncertainty in the estimation of thickness natural log is taken on both sides of equation (4) and is then differentiated,

$$\frac{dH}{H} = \frac{du_s}{u_s} - \frac{du_b}{u_b} - \frac{dA}{A} - \frac{df}{f} - \frac{d\rho}{\rho} - \frac{dg}{g} - \frac{d\alpha}{\alpha} \quad (5)$$

Further slope dependent approach proposed by Haeberli and Hoelzle 1995 [9] is also used for obtaining mean ice-thickness using the following equation.

$$\tau_b = \rho g h_f \sin \alpha \quad (6)$$

where  $h_f$  is the mean ice thickness along the central flow line. It uses average surface slope and the vertical extent of the glacier for estimating the mean glacier thickness and hence glacier volume.

The foundation for the parameterization scheme [19] consists of measured inventory data on the total length ( $L_0$ ), maximum and minimum altitude ( $H_{max}$ ,  $H_{min}$ ) and total surface area ( $F$ ) of the investigated glacier. For Janapa-Garang glacier, values of  $L_0 = 7.40 \text{ km}$ ,  $H_{max} = 5640 \text{ m}$ , and  $H_{min} = 4220 \text{ m}$  are taken from GSI glacier inventory 1999. From these basic parameters, mean altitude ( $H_m = [H_{max} - H_{min}] / 2$ ), vertical extent ( $\Delta H = H_{max} - H_{min}$ ) and average surface slope ( $\alpha = \arctan [\Delta H / L_0]$ ) are derived in the first step. The ice density  $\rho$  is assigned a constant value of  $900 \text{ kg m}^{-3}$  [8],  $g$  is the acceleration due to gravity and has value  $9.8 \text{ m s}^{-2}$ ,  $f$  is the scale factor or shape factor i.e. the ratio between the driving stress and basal stress along the glacier and it ranges between 0.8-1 for temperate glaciers [9]. For the present study 0.8 is used as it is a typical value for valley glaciers [4]. The parameterization of average basal shear stress ( $\tau_b$ ) concerning elevation range  $\Delta H$  (km) depends on the reconstructed Pleistocene glaciers of European Alps. [9].

Usefulness of remote-sensing and ..... volume of glacier

$$\tau \text{ [kPa]} = \{ 0.5 + 159.8\Delta H - 43.5(\Delta H)^2 : \Delta H \leq 1.6 \text{ km} \text{ (7)}$$

$$= \{ 150 : \Delta H > 1.6 \text{ km}$$

From equation (7) the value of  $\tau_b$  for Janapa-Garang glacier is 138.96 kPa.

Mean ice thickness along the central flow line ( $h_f$ ) is extrapolated for the entire glacier assuming that glacier has semi-elliptical cross-sectional geometry [9]. The  $h_f$  is then multiplied by for obtaining the mean ice thickness for the entire glacier.

$$h_F = h_f \text{ (8)}$$

The third approach used for estimating ice-thickness is a depth-area scaling approach, proposed by Chaohai et al. 1988 [15]. The depth here is calculated by substituting the area of the glacier in the following empirical equation

$$\text{Depth (m)} = -11.32 + 53.21 * (\text{Area})^{0.3} \text{ (9)}$$

Additionally, an attempt has been made to estimate volume from the thickness values obtained from slope-dependent approach and depth-area approach, simply by taking the product of area and depth; with the only purpose of comparison (Table 2).

(c) Estimation of volume:

Volume-area scaling is a widely used approach for estimating the ice volume because of its easy and fast application. Once the scaling parameters are determined, glacier volume can be quickly computed for the glacier with known area [11]. The general form of V–A scaling relation is:

$$V = cA^{\gamma} \text{ (10)}$$

where,  $V$  = glacier volume

$A$  = glacier area,  $c$  and  $\gamma$  = scaling parameters

Following are three V-A approaches with their scaling parameters used in the current study:

(a) Bahr et al. Method (1997):

$$\text{Volume (m}^3\text{)} = 0.191 \times (\text{Area})^{1.375} \quad (11)$$

(b) Chen & Ohmura et al. Method (1990):

$$\text{Volume (m}^3\text{)} = 0.2055 \times (\text{Area})^{1.35} \quad (12)$$

(c) Arendt et al. Method:

$$\text{Volume (m}^3\text{)} = 0.28 \times (\text{Area})^{1.375} \quad (13)$$

#### 4. Results and Discussion

Surface velocities for Janapa-Garang glacier are shown in (Figure 5). Velocity peaks in the inner portion of the glacier reaching up-to value of  $\sim 28\text{m/yr}$  for glacier-1 and  $\sim 21\text{m/yr}$  for the glacier-2, and progressively decreases to  $\sim 0.6\text{ m/yr}$  for glacier-1 and  $\sim 0.1\text{ m/yr}$  for glacier-2 towards the peripheral regions of the glacier and the snout. Higher velocities at places in the lower reaches could be attributed to heterogeneity in topographic parameters such as slope, aspect and curvature [20].

Ice-thickness and volume computed from the different approaches described earlier are presented in table 2. Uncertainty in thickness is estimated to be 4.196 m from equation (5).

In the case of Janapa-Garang glacier, no field estimates of surface velocity are available to validate. However, in past similar studies have been carried out on Gangotri glacier, PRG glacier, Chhotashighri glacier and results of same are matching with field data [1], [6-7]. However, computed thickness values particularly from Slope-dependent approach and Laminar flow equation; and volume particularly using scaling parameters of Bahr et al. 1997 [13] are closely comparable with the published field estimates for thickness and volume i.e. 70 m and 0.70 km<sup>3</sup> respectively [25].

#### Conclusions

We have estimated the surface velocities using COSI-Corr algorithm, ice-thickness using laminar flow equation, slope-dependent approach and depth-area scaling method. Also, we have an estimated volume using the volume-area scaling relationships. These techniques provide wide-field coverage, automated workflows, generate the most accurate results and are highly viable from

monitoring the dynamic parameters of the glacier. Variations in the velocity values are observed in different parts of the glacier. The spatial distribution of surface velocity for Janapa-Garang glacier is similar to the studies carried out by other workers on Gangotri, PRG, ChottaShigri [1], [6-7]. (Figure 6) represents the volume and thickness estimates obtained by applying different approaches. Results of thickness obtained from Slope-dependent approach and Laminar flow equation; and volume from scaling parameters of Bahr et al. 1997 [13] are closely comparable to the published field values [25]. Hence, the aforesaid techniques to obtain thickness and volume are most suitable for glaciers with an extent similar to Janapa-Garang glacier. Thus, the present study points the strength of remote sensing and geospatial tools in conducting the glaciological studies in areas of inclement weather conditions such as in the Himalayas and other parts of the world.

### Acknowledgement

Authors are thankful to Head, Department of Geology, The M.S. University of Baroda for providing the necessary infrastructural facilities. The first author wishes to place on record Dr. A.V. Kulkarni, distinguished scientist, Divecha Centre for Climate Change, IISc Bangalore for allowing him to attend the training on glacier studies and remote sensing.

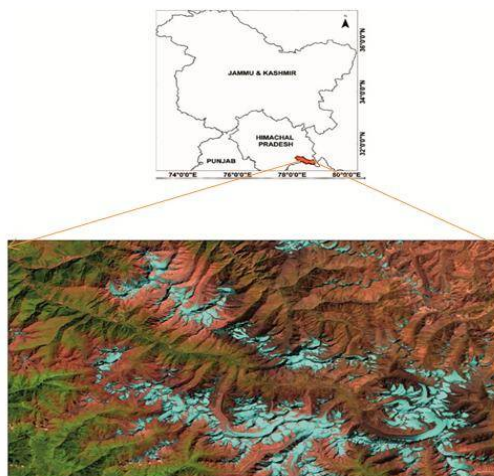
### References

- [1] Gantayat, P., Kulkarni, A.V. and Srinivasan, J., 2014. Estimation of ice thickness using surface velocities and slope: case study at Gangotri Glacier, India. *Journal of Glaciology*, 60(220), pp.277-282.
- [2] Berthier, E., Raup, B. and Scambos, T., 2003. New velocity map and mass-balance estimate of Mertz Glacier, East Antarctica, derived from Landsat sequential imagery. *Journal of Glaciology*, 49(167), pp.503-511.
- [3] Stocker-Waldhuber, M., Fischer, A., Helfricht, K. and Kuhn, M., 2018. Ice flow velocity as a sensitive indicator of glacier state. *The Cryosphere Discuss.*, <https://doi.org/10.5194/tc-2018-37>, in review.
- [4] Haq, M.A., Jain, K. and Menon, K.P.R., 2014. Modelling of Gangotri glacier thickness and volume using an artificial neural network. *International journal of remote sensing*, 35(16), pp.6035-6042.
- [5] Gao, J. and Liu, Y., 2001. Applications of remote sensing, GIS and GPS in glaciology: a review. *Progress in Physical Geography*, 25(4), pp.520-540.

- [6] Tiwari, R.K., Gupta, R.P. and Arora, M.K., 2014. Estimation of surface ice velocity of Chhota-Shigri glacier using sub-pixel ASTER image correlation. *Current Science*, pp.853-859.
- [7] Jawak, S.D., Kumar, S., Luis, A.J., Bartanwala, M., Tummala, S. and Pandey, A.C., 2018. Evaluation of Geospatial Tools for Generating Accurate Glacier Velocity Maps from Optical Remote Sensing Data. In *Multidisciplinary Digital Publishing Institute Proceedings* (Vol. 2, No. 7, p. 341).
- [8] Farinotti, D., Huss, M., Bauder, A. and Funk, M., 2009. An estimate of the glacier ice volume in the Swiss Alps. *Global and Planetary Change*, 68(3), pp.225-231.
- [9] Haeberli, W. and Hölzle, M., 1995. Application of inventory data for estimating characteristics of and regional climate-change effects on mountain glaciers: a pilot study with the European Alps. *Annals of glaciology*, 21, pp.206-212.
- [10] Cuffey, K.M. and Paterson, W.S.B., 2010. *The physics of glaciers*. Academic Press.
- [11] Frey, H., Machguth, H., Huss, M., Huggel, C., Bajracharya, S., Bolch, T., Kulkarni, A., Linsbauer, A., Salzmann, N. and Stoffel, M., 2014. Estimating the volume of glaciers in the Himalayan–Karakoram region using different methods. *The Cryosphere*, 8(6), pp.2313-2333.
- [12] Radić, V., Hock, R. and Oerlemans, J., 2008. Analysis of scaling methods in deriving future volume evolutions of valley glaciers. *Journal of glaciology*, 54(187), pp.601-612.
- [13] Bahr, D.B., 1997. Width and length scaling of glaciers. *Journal of Glaciology*, 43(145), pp.557-562.
- [14] Leprince, S., Barbot, S., Ayoub, F. and Avouac, J.P., 2007. Automatic and precise orthorectification, coregistration, and subpixel correlation of satellite images, application to ground deformation measurements. *IEEE Transactions on Geoscience and Remote Sensing*, 45(6), pp.1529-1558.
- [15] Chaohai, L. and Sharma, C.K., 1988. Report on first expedition to glaciers in the Pumqu (Arun) and Poiqu (Bhote-Sun Kosi) river basins, Xizang (Tibet), China.
- [16] Chen, J. and Ohmura, A., 1990. Estimation of Alpine glacier water resources and their change since the 1870s. *IAHS publ*, 193, pp.127-135.
- [17] Arendt, A.A., Echelmeyer, K.A., Harrison, W.D., Lingle, C.S. and Valentine, V.B., 2002. Rapid wastage of Alaska glaciers and their contribution to rising sea level. *Science*, 297(5580), pp.382-386.
- [18] Swaroop S, Raina VK and Sangeswar CV (2003) Ice flow of Gangotri glacier. In Srivastava D, Gupta KR and Mukerji S eds. *Proceedings of the Workshop on Gangotri glacier, 26–28 March 2003, Lucknow, India*. (Spec. Publ. 80) Geological Survey of India, Kolkata.
- [19] Hölzle, M., 1994. *Permafrost und GletscherimOberengadin: Grundlagen und AnwendungsbeispielefürautomatisierteSchätzverfahren* (Doctoral dissertation, ETH Zurich).

Usefulness of remote-sensing and ..... volume of glacier

- [20] Sam, L., Bhardwaj, A., Kumar, R., Buchroithner, M.F. and Martín-Torres, F.J., 2018. Heterogeneity in topographic control on velocities of Western Himalayan glaciers. *Scientific reports*, 8(1), pp.1-16.
- [21] Haeberli, W., Frauenfelder, R., Hoelzle, M. and Maisch, M., 1999. On rates and acceleration trends of global glacier mass changes. *Geografiska Annaler: Series A, Physical Geography*, 81(4), pp.585-591.
- [22] Boko, M., Niang, I., Nyong, A., Vogel, A., Githeko, A., Medany, M., Osman-Elasha, B., Tabo, R. and Yanda, P.Z., 2018. Africa Climate Change 2007: Impacts, Adaptation and Vulnerability: Contribution of Working Group II to the Fourth Assessment Report of the Intergovernmental Panel on Climate Change.
- [23] Oerlemans, J., 2005. Extracting a climate signal from 169 glacier records. *Science*, 308(5722), pp.675-677.
- [24] Paul, F., Kääb, A. and Haeberli, W., 2007. Recent glacier changes in the Alps observed by satellite: Consequences for future monitoring strategies. *Global and Planetary Change*, 56(1-2), pp.111-122.
- [25] Geological survey of India,(1999). Inventory of the Himalayan glaciers, a contribution to International Hydrological program. Geol. Surv. India. Sp. Pub. (Ed. M.K. Kaul), 34, 165 p.

**Tables and figures:**

**Figure 1. Location Map of Baspa Basin, Himachal Pradesh, India. Landsat-8 Image; Composite of SWIR, NIR and Green Band.**

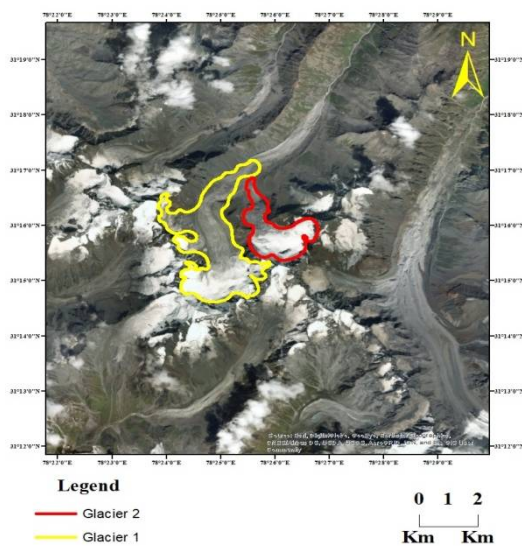


**Figure 2. Google earth image of Janapa-Garang glacier**

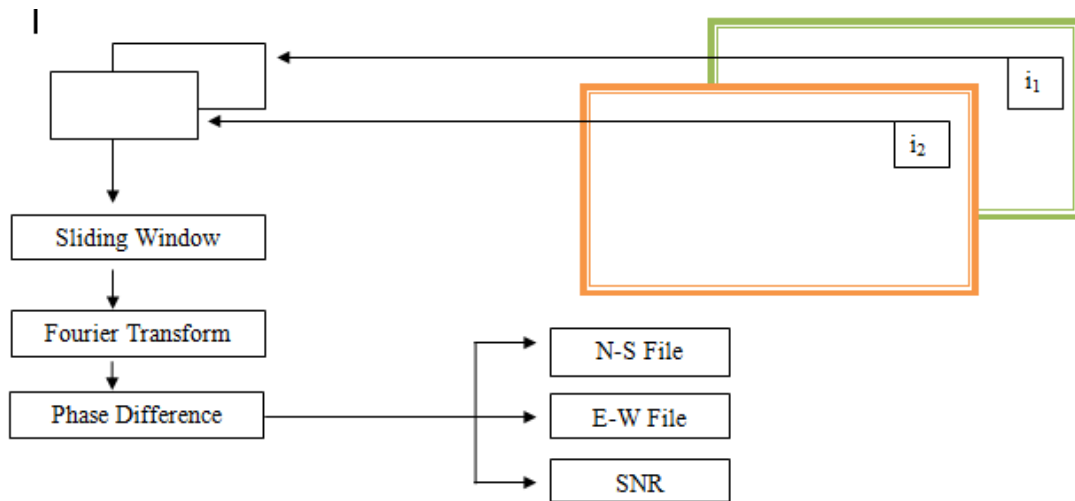


**Figure 3. COSI-Corr Working**

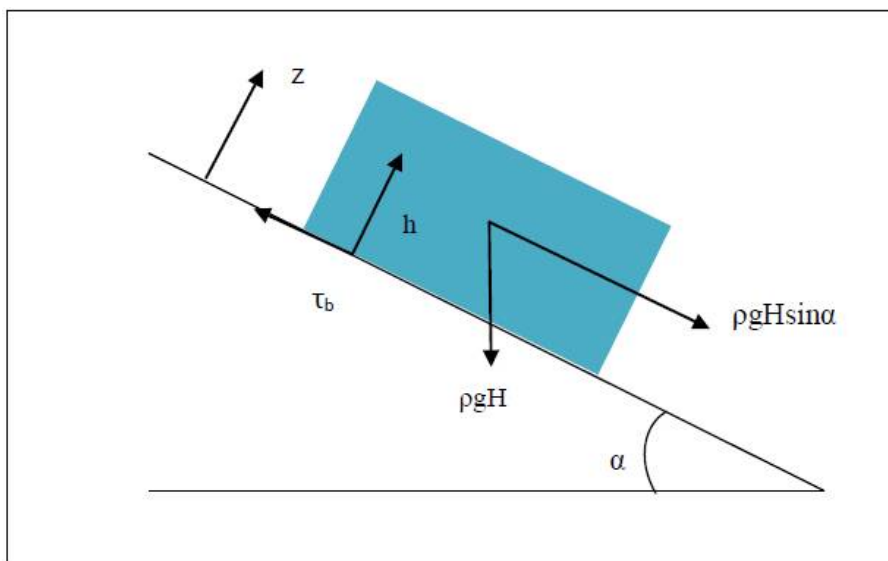


**Figure 4. Simplified model of glacier considered in laminar flow equation**

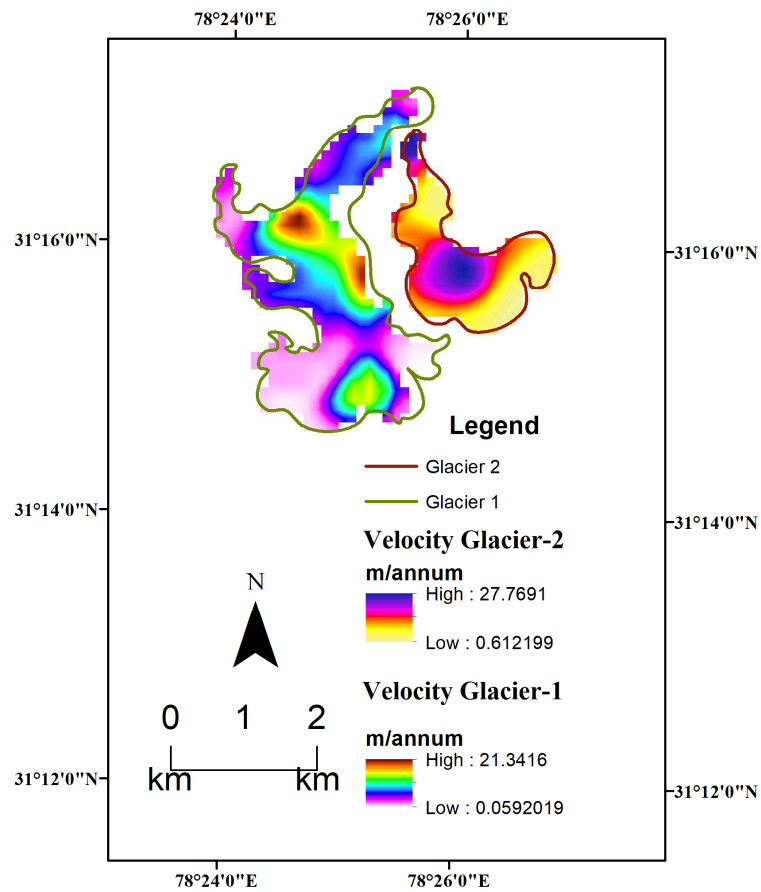


**Figure 5. Surface Velocity Field for Janapa-Garang Glacier**

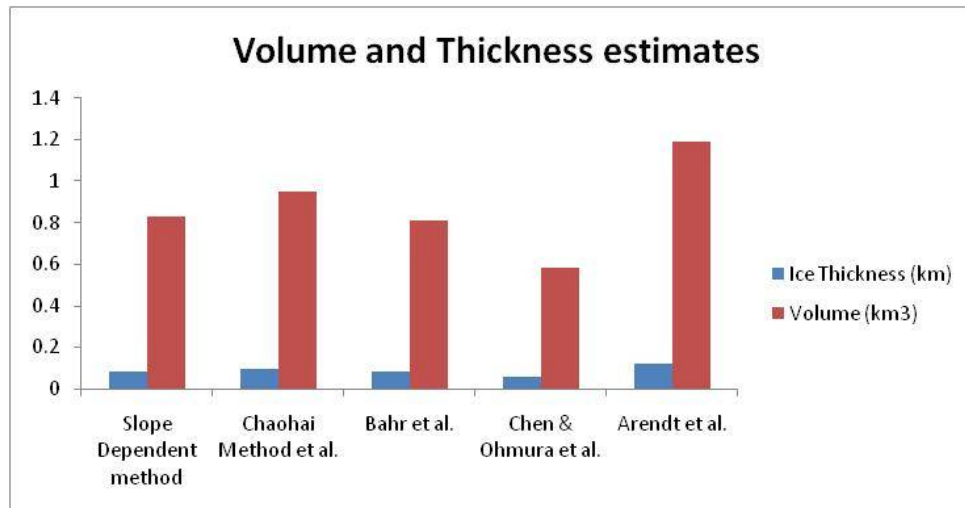


Figure 6. Volume and thickness estimates obtained from different approaches

Table 1. Details of datasets used in the study

Serial no.	Satellite name	Sensor name	Resolution	Date of aquisition
1	Landsat 8	OLI_TIRS	30 m, 15 m	09-26-2016
2	Landsat 8	OLI_TIRS	30 m, 15 m	09-29-2017
<b>Path : 146 Row: 38 Map Projection &amp; projection unit: UT meters Datum: WGS84 Zone: 44</b>				

Table 2. Volume and Ice thickness obtained from different approaches

Serial No.	Method	Ice-thickness (m)	Volume (km <sup>3</sup> )
1	Laminar Flow Equation	82.89 m $\pm$ 4.196 m	---
2	Slope Dependent method	82.66	0.83
3	Chaohai Method et al.	95.10	0.95
4	Bahr et al.	80.75	0.814
5	Chen & Ohmura et al.	58.03	0.585
6	Arendt et al.	118.05	1.19

-----

# A BAYESIAN APPROACH TO THE OPTIMAL WARRANTY LENGTH FOR PARETO DISTRIBUTED PRODUCT WITH MULTIPLY TYPE-II CENSORING SCHEME

**D. T. Patel<sup>1</sup>, M. N. Patel<sup>2</sup>**

<sup>1</sup>SLU Arts and H and P Thakor Commerce College,  
Ellisbridge, Ahmedabad-380006;

<sup>2</sup>Department of Statistics, School of Sciences, Gujarat University,  
Ahmedabad-380009;

Email: divyapatel.1985@yahoo.com

Email: mnpatel.stat@gmail.com

## **Abstract**

In this paper we use a Bayesian approach to determine the optimal warranty lengths. The optimal warranty is that which maximizes the expected utility of the product. The Pareto distribution is employed to describe the product life time under multiply type-II censoring scheme. We have considered a combination of free replacement policy and pro-rata policy for the warranty. A numerical data is used to exemplify the theory. A sensitivity study is carried out to check the effect of hyper parameters on the optimal warranty length and the optimal value of expected utility.

**Keywords:** Posterior distribution, warranty policy, economic benefit function, warranty cost function, dissatisfaction cost function, multiply Type-II censoring.

## **1. Introduction**

In an intensively competitive market one way by which manufacturers attract consumers to their products is by providing warranties on products. The major goal of the manufacturing firms is of increasing profits. The sales volume and warranty are the important factors of marketing products. The sales volume of the product depends on the selling price and quality of the product. A good quality product requires some more cost, which increases the selling price of the product (Scitovszky[1]). Quality of the product can be predicted based on its warranty. Through warranties, customers are provided guarantees for failure free, acceptable service for a period of time following the purchase of product. In general, buyers believe that a product with a long warranty period is higher quality, and more

reliable than the one with a short warranty period. For manufacturers, a warranty program is an important tool in marketing products. It not only serves as a sales weapon to increase the sales volume, but also brings considerable profits. However, if the product quality is low, it can be expensive.

Thus, a proper warranty plays important role in increasing sale volume of the products. Warranty is an important factor of marketing products because a better warranty policy usually signals the higher product quality and provides greater assurance to customers. Warranty always involves additional costs to the producer and these costs depend on product reliability. Many authors have contributed in the area of warranty length some of them are Blischke and Murthy[2], Singpurwalla and Wilson[3], Huang et al[4]. If the manufacturers wish to give compensation to the buyer when failure occurs, the warranty length and the reliability of the product play a key role on determining the cost of the product. Wu and Huang[5] have considered optimal warranty length in case of the product having Rayleigh distributed life time. The Rayleigh distribution has an increasing failure rate over a time. Wu et al[6] also have considered normal distribution as a product life time model which is suitable when the product possesses increasing failure rate. In the existing literature the work related to optimal warranty has not been done on the basis of life time models other than Rayleigh and Normal. Life time of product may follow various types of life time distributions like Exponential, Power function, Kumaraswamy etc. In this paper we have considered Pareto life time model for the product having decreasing failure rate.

A manufacturer must have some information about product reliability to design a cost-effective warranty. Censoring is very common in life tests. It is used to save cost and time. In failure data analysis is common that some individuals cannot be observed for the full time to failure. For example, in the familiar Type-II censoring, observation ceases after a predetermined number of failures may be for reasons of economy perhaps. Multiply Type-II censoring is a useful and more general scheme in which a specific number of individuals at risk may be removed from the study at or after several ordered failure times. This allowance will be desirable, as in the case of accidental breakage of experimental units, in which the loss of test units at points often than the termination point may be unavoidable. Hence intermediate removal may also be desirable when a compromise between reduced time of experimentation and the observation of at least some extreme

lifetimes is sought. In some reliability experiments, an experimenter may decide that it is inappropriate or too dangerous to carry on the testing on some of the tested units even though these units have not failed. These reasons lead us into the area of multiply type-II censoring. Statistical inference under censoring has received the attention of many authors. Articles by Cohen[7], Mann[8], and Viveros et al.[9], Gouno et al[10], Patel and Patel[11], Gajjar and Patel[12] are some early works on estimation under different types of censoring schemes.

The aim of this paper is to determine optimal warranty length for the product having Pareto life time distribution. The information of product reliability is obtained through a multiply type-II censored life test. To determine optimal warranty period utility function is used, the concept of utility function is considered by Wu and Huang[5]. In Section 2 the likelihood function for the Pareto distribution is constructed based on multiply type-II censored sample. Using gamma conjugate prior distribution for the parameter of the life time distribution its posterior distribution is obtained. A posterior predictive distribution is derived using the posterior distribution. Section 3 gives the warranty policies. A combined warranty policy based on FRW and PRW are described. Cost functions under the above warranty policies are obtained using the concept of Wu and Huang[5]. Section 4 provides utility function which is constructed using economic benefit function, warranty cost function and dissatisfaction cost. Section 5 covers the maximization of expected utility function and optimal warranty. In Section 6 a numerical example is given. The economic sensitivity analysis is also carried out in Section 7 to evaluate the effect of the prior parameters. Some conclusions are drawn in Section 8.

## 2. Life time model and posterior distribution

The Pareto distribution has its own importance in the life testing experiments. This distribution is considered by many authors like Aggarwala and Childs[13], Arnold[14], Chareti[15], Hossain and Zimmer[16], Mahmmd et al.[17], Podder et al.[18], Shah and Patel[19].

The probability density function of Pareto distribution is given by

$$f(x|\theta) = \theta x^{-\theta-1}, x \geq 1, \theta > 0 \quad ..(2.1)$$

Its cumulative distribution function is given by of

$$F(x|\theta) = 1 - x^{-\theta}, x \geq 1, \theta > 0$$

It is very common that the lifetimes of some test units may not be able to be recorded exactly. In this paper we have used multiply type-II censoring scheme as considered by Upadhyay et al[20].

Suppose  $n$  units are put on a life test and the first  $r$ , middle  $l$  and last  $s$  observations are censored that is only ordered observations are  $X_{r+1}, X_{r+2}, \dots, X_{r+k}$  and  $X_{r+k+l+1}, X_{r+k+l+2}, \dots, X_{n-s}$  are observed. The scheme is known as the multiply type-II censoring scheme. The other version of Multiply Type-II censoring has been considered by many authors such as Balakrishnan[21], Balasubramanian and Balakrishnan[22], Singh and Kumar[23], Shah and Patel[24]. This censoring scheme is useful in follow-up studies in epidemiology, reliability and endocrinology.

The general form of the likelihood function based on the abovemultiply type-II censoring is given by

$$\begin{aligned} L(\theta, x) &= \frac{n!}{r!l!m!} (F(x_{r+1}))^r \prod_{i=r+1}^{r+k} f(x_i) (F(x_{r+k+l+1}) - F(x_{r+k}))^l \prod_{i=r+k+l+1}^{n-m} f(x_i) [1 - \\ &F(x_{n-m})]^m \\ &= c(1 - e^{-\theta x_{r+1}})^r \theta^k e^{-\theta \sum_{i=r+1}^{r+k} x_i} [e^{-\theta x_{r+k}} - e^{-\theta x_{r+k+l+1}}]^{l+1} \theta^{n-m-r-k-1} \times \\ &e^{-\theta \sum_{i=r+k+l+1}^{n-m} x_i} (e^{-\theta x_{n-m}})^m \end{aligned} \quad ..(2.1)$$

where  $c = \frac{n!}{r!l!m!}$  The most widely suitable prior for the parameter  $\theta$  of the exponential distribution is the gamma conjugate prior. The gamma conjugate prior for  $\theta$  is given by

$$\pi(\theta) = \frac{\delta^v}{\Gamma(v)} \theta^{v-1} e^{-\delta\theta}; \theta > 0, \delta > 0, v > 0 \quad ..(2.3)$$

The posterior distribution of the parameter  $\theta$  can be obtained as

$$\begin{aligned} \pi(\theta|x) &= \frac{L(\theta, x)\pi(\theta)}{\int_0^\infty L(\theta, x)\pi(\theta)d\theta} \\ &= \frac{\theta^{n_1-2} \sum_{j=0}^l \sum_{i=0}^r e^{-\theta(\delta-s_{ij})} h_1(j) h_2(i)}{\Gamma(n_1-1) \sum_{j=0}^l \sum_{i=0}^r \frac{h_1(j) h_2(i)}{(\delta-s_{ij})^{n_1-1}}} \end{aligned} \quad ..(2.4)$$

where

$$s_2 = \sum_{z=r+1}^{r+k} \log x_z + \sum_{z=r+k+l+1}^{n-m} \log x_z, h_1(j) = \binom{l}{j} (-1)^{l-j}, h_2(i) = \binom{r}{i} (-1)^{r-i},$$

$$s_{ij} = - \sum_{z=r+1}^{r+k} \log x_z - \sum_{z=r+k+1+1}^{n-m} \log x_z - l \log x_{r+k+1+1} - m \log x_{n-m} + j \log \left( \frac{x_{r+k+1+1}}{x_{r+k}} \right) - i \log x_{r+1}$$

Using (2.1) and (2.4) the posterior predictive distribution can be obtained as

$$\begin{aligned} f(t|x) &= \int_0^\infty f(t|\theta) \pi(\theta|x) d\theta \\ &= \int_0^\infty \theta t^{-\theta-1} \frac{\theta^{n_1-2} \sum_{j=0}^l \sum_{i=0}^r e^{-\theta(\delta-s_{ij})} h_1(j) h_2(i)}{\Gamma(n_1-1) \sum_{j=0}^l \sum_{i=0}^r \frac{h_1(j) h_2(i)}{(\delta-s_{ij})^{n_1-1}}} d\theta \\ &= \frac{(n_1-1) \sum_{j=0}^l \sum_{i=0}^r \frac{h_1(j) h_2(i)}{(\delta-s_{ij} + \log t)^{n_1}}}{t \sum_{j=0}^l \sum_{i=0}^r \frac{h_1(j) h_2(i)}{(\delta-s_{ij})^{n_1-1}}} \end{aligned} \quad ..(2.5)$$

The posterior predictive cumulative distribution is given by

$$\begin{aligned} F(w|x) &= \int_1^w f(t|x) dt \\ &= \int_1^w \frac{(n_1-1) \sum_{j=0}^l \sum_{i=0}^r \frac{h_1(j) h_2(i)}{(\delta-s_{ij} + \log t)^{n_1}}}{t \sum_{j=0}^l \sum_{i=0}^r \frac{h_1(j) h_2(i)}{(\delta-s_{ij})^{n_1-1}}} dt \\ &= \frac{\sum_{j=0}^l \sum_{i=0}^r h_1(j) h_2(i) [(\delta-s_{ij})^{-n_1+1} - (\delta-s_{ij} + \log w)^{-n_1+1}]}{\sum_{j=0}^l \sum_{i=0}^r \frac{h_1(j) h_2(i)}{(\delta-s_{ij})^{n_1-1}}} \end{aligned} \quad ..(2.6)$$

Now consider the integration

$$\begin{aligned} I &= \int_{l_1}^{u_1} t f(t|x) dt = \int_{l_1}^{u_1} t \frac{(n_1-1) \sum_{j=0}^l \sum_{i=0}^r \frac{h_1(j) h_2(i)}{(\delta-s_{ij} + \log t)^{n_1}}}{t \sum_{j=0}^l \sum_{i=0}^r \frac{h_1(j) h_2(i)}{(\delta-s_{ij})^{n_1-1}}} dt \\ &= \frac{(n_1-1) \sum_{j=0}^l \sum_{i=0}^r h_1(j) h_2(i) I_0}{\sum_{j=0}^l \sum_{i=0}^r \frac{h_1(j) h_2(i)}{(\delta-s_{ij})^{n_1-1}}} \end{aligned} \quad ..(2.7)$$

where,

$$I_0 = \int_{l_1}^{u_1} (\delta - s_{ij} + \log t)^{-n_1} dt$$

for which we do not have a simplification in the closed form, so we can use numerical integration during its calculation.

### 3. Warranty Policy

Here we have considered a combination of the two commonly used warranty policies namely free replacement warranty (FRW) and pro-rata warranty (PRW). Under FRW policy, if a product fails during the warranty period, the product is replaced by another product of the same kind free of charge.

Under PRW policy the manufacturer gives compensation to the buyer, which may be a linear function of the remaining time of the warranty linear function of the warranty period.

A combination of these two types of policies is called FRW/PRW policy.

Here we assume FRW during the period  $[0, w_1)$ , and for PRW during the period  $[w_1, w_2)$ ,  $w_1 \leq w_2$  are positive values. The reimbursing cost function of an item with time length  $t$  for combined FRW/ PRW policy is given by

$$C_w(t) = \begin{cases} S, & 0 \leq t < w_1 \\ S \left( \frac{w_2 - t}{w_2 - w_1} \right), & w_1 \leq t < w_2 \\ 0, & t \geq w_2 \end{cases} \quad \text{..(3.1)}$$

and in case of FRW policy ( $w_1=w_2$ ) cost function is given by,

$$C_w(t) = \begin{cases} S, & 0 \leq t < w_1 \\ 0, & t \geq w_1 \end{cases} \quad \text{..(3.2)}$$

and under PRW policy ( $w_1=0$ ) cost function is given by

$$C_w(t) = \begin{cases} S \left( \frac{w_2 - t}{w_2} \right), & 0 \leq t < w_2 \\ 0, & t \geq w_2 \end{cases} \quad \text{..(3.3)}$$

where  $S$  is the selling price of the product which is cost to the buyer.

This cost function is also called the manufacturer loss associated with setting up a warranty.

### 4. Utility Function

In the combined FRW/PRW policy, the warranty length, say  $w_1, w_2$  are determined for a product. To determine the values of  $w_1$  and  $w_2$  one has to consider a

function of warranty policy that measures the monetary utility when the product fails at time t.

Here we consider the utility function used by Wu and Huang[5] based on the economic benefit function  $B(w_1, w_2)$ , the warranty cost function  $W(w_1, w_2)$  and the dissatisfaction cost function  $D(t, w_1, w_2)$  defined as

$$U(t, w_1, w_2) = B(w_1, w_2) - W(w_1, w_2) - D(t, w_1, w_2) \quad ..(4.1)$$

Here economic benefit function is proposed as

$$B(w_1, w_2) = A_1 M \left( 1 - e^{-A_2 \left( \frac{w_1 + w_2}{2} \right)} \right) \quad ..(4.2)$$

Where  $A_1$  is the profit per product obtained by manufacturer and  $M$  is the potential number of products to be sold with this warranty policy. The parameter  $A_2$  controls the speed of increment in benefit. The ratio shows the percentage of benefit remains when the manufacturer changes the warranty from FRW to PRW.

$$\frac{B(0, t_w)}{B(t_w, t_w)} = \frac{1 - e^{-\frac{A_2 t_w}{2}}}{1 - e^{-A_2 t_w}} \quad ..(4.3)$$

By solving (4.3), the value of the parameter  $A_2$  can be derived.

The warranty cost function  $W(t, w_1, w_2)$  is an item  $C_w(t)$  times the expected number of items that fail under the warranty period. The expected number of failures can be determined using the method given by Wu and Huang[5] based on the posterior predictive cumulative distribution function  $F(\cdot | x)$  as shown below,

$$\text{The expected number of failures} = \begin{cases} MP(0 < t < w_1), & 0 \leq t < w_1 \\ MP(w_1 \leq t < w_2), & w_1 \leq t < w_2, \\ MP(t \geq w_2), & t \geq w_2 \end{cases}$$

Hence, the warranty cost function can be written as

$$W(t, w_1, w_2) = MF(w_1|x)S I_{[0, w_1)}(t) + M[F(w_2|x) - F(w_1|x)]S \left( \frac{w_2-t}{w_2-w_1} \right) I_{[w_1, w_2)}(t) \quad ..(4.4)$$

The dissatisfaction cost is the manufacturer's indirect cost, when the product fails during the warranty period, or fails during time just after warranty, such cost function is used by Patankar et al[25] and Kelly et al[26]. Under the combined FRW/PRW policy the dissatisfaction cost function considered by Wu and Huang[5] as

$$D(t, w_1, w_2) = D_1(t, w_1) + D_2(t, w_1, w_2) + D_3(t, w_2) \quad ..(4.5)$$

In case of FRW policy, when product fails in the time period  $[0, w_1)$ , the dissatisfaction cost is a proportion  $q_1$  ( $0 < q_1 < 1$ ) of the sales price  $S$ , multiplied by the expected number of failures,

$$D_1(t, w_1) = NF(w_1|x)Sq_1 I_{[0, w_1)}(t)$$

The second component is for the product fails during the time interval  $[w_1, w_2)$ . Here it is assumed that the dissatisfaction cost of an item linearly decreased with time with maximum  $Sq_1$  and minimum  $Sq_2$ ,  $0 < q_2 < q_1 < 1$ .

Hence,

$$D_2(t, w_1, w_2) = M[F(w_2|x) - F(w_1|x)] \left[ Sq_1 - (Sq_1 - Sq_2) \left( \frac{t-w_1}{w_2-w_1} \right) \right] I_{[w_1, w_2)}(t)$$

And the third component  $D_3(t, w_2)$  is for the product fails after the expiration of warranty, but the customer may still be unsatisfied with the product unless its lifetime exceeds a specified value  $L$ ,  $L > w_2$  here  $D_3(t, w_2)$  decreases linearly with time  $t$ , reaching to zero when lifetime is  $L$  and given by

$$D_3(t, w_2) = M[F(L|x) - F(w_2|x)]Sq_2 \left( \frac{L-t}{L-w_2} \right) I_{[w_2, L)}(t)$$

The value of  $L$  may be considered as the mean or median or percentile of the posterior predictive distribution given in (2.5).

### 5. Optimal Warranty

The optimal warranty  $(w_1^*, w_2^*)$  is that which maximize the expected value of the utility function EU with expectation over the posterior predictive distribution, That is

$$E(U(T, w_1, w_2)) = \int_0^\infty U(T, w_1, w_2) f(t|x) dt \quad ..(5.1)$$

Using (4.1) and (2.5) in (5.1), we get the expression for the expected utility function as

$$\begin{aligned} E(U(T, w_1, w_2)) &= \int_0^\infty \{B(w_1, w_2) - W(w_1, w_2) - D(t, w_1, w_2)\} f(t|x) dt \\ &= I_1 - I_2 - I_3 \end{aligned} \quad ..(5.2)$$

where

$$\begin{aligned} I_1 &= \int_0^\infty B(w_1, w_2) f(t|x) dt \\ &= A_1 M(1 - e^{-A_2 (\frac{w_1 + w_2}{2})}) \end{aligned} \quad ..(5.3)$$

$$I_2 = \int_0^\infty W(w_1, w_2) f(t|x) dt$$

Using (4.4), we can simplify as

$$\begin{aligned} I_2 &= M[S[F(w_1|x)]^2 - S[F(w_2|x) - F(w_1|x)][I_{2.1} - I_{2.2}]] \\ &= MS \left[ \frac{\sum_{j=0}^1 \sum_{i=0}^r h_1(j) h_2(i) [(\delta - s_{ij})^{-n_1+1} - (\delta - s_{ij} + \log w_1)^{-n_1+1}]}{\sum_{j=0}^1 \sum_{i=0}^r \frac{h_1(j) h_2(i)}{(\delta - s_{ij})^{n_1-1}}} \right]^2 \\ &\quad - MS \left[ \frac{\sum_{j=0}^1 \sum_{i=0}^r h_1(j) h_2(i) [(\delta - s_{ij} + \log w_2)^{-n_1+1} - (\delta - s_{ij} + \log w_1)^{-n_1+1}]}{\sum_{j=0}^1 \sum_{i=0}^r \frac{h_1(j) h_2(i)}{(\delta - s_{ij})^{n_1-1}}} \right] (I_{2.1} - I_{2.2}) \end{aligned} \quad ..(5.4)$$

where

$$\begin{aligned}
I_{2.1} &= \frac{w_2}{w_2 - w_1} \int_{w_1}^{w_2} f(t|x) dt \\
&= \frac{w_2}{w_2 - w_1} [F(w_2|x) - F(w_1|x)] \\
&= \frac{w_2}{w_2 - w_1} \left[ \frac{\sum_{j=0}^l \sum_{i=0}^r h_1(j) h_2(i) [(\delta - s_{ij} + \log w_2)^{-n_1+1} - (\delta - s_{ij} + \log w_1)^{-n_1+1}]}{\sum_{j=0}^l \sum_{i=0}^r \frac{h_1(j) h_2(i)}{(\delta - s_{ij})^{n_1-1}}} \right]
\end{aligned}$$

$$I_{2.2} = \frac{1}{w_2 - w_1} \int_{w_1}^{w_2} t f(t|x) dt$$

Using the result (2.7) we have

$$I_{2.2} = \frac{1}{w_2 - w_1} \left[ \frac{(n_1 - 1) \sum_{j=0}^l \sum_{i=0}^r h_1(j) h_2(i) I_{12}}{\sum_{j=0}^l \sum_{i=0}^r \frac{h_1(j) h_2(i)}{(\delta - s_{ij})^{n_1-1}}} \right]$$

where,

$$I_{12} = \int_{w_1}^{w_2} (\delta - s_{ij} + \log t)^{-n_1} dt$$

Now,

$$I_3 = \text{MSq}_1 [F(w_1|x)]^2 - \text{MS} [F(w_1|x) - F(w_1|x)] (I_{3.1} - I_{3.2}) - \text{MSq}_2 [F(L|x) - F(w_2|x)] (I_{3.3} - I_{3.4})$$

$$\begin{aligned}
&= \text{MSq}_1 \left[ \frac{\sum_{j=0}^l \sum_{i=0}^r h_1(j) h_2(i) [(\delta - s_{ij})^{-n_1+1} - (\delta - s_{ij} + \log w_1)^{-n_1+1}]}{\sum_{j=0}^l \sum_{i=0}^r \frac{h_1(j) h_2(i)}{(\delta - s_{ij})^{n_1-1}}} \right]^2 \\
&\quad - \text{MS} \left[ \frac{\sum_{j=0}^l \sum_{i=0}^r h_1(j) h_2(i) [(\delta - s_{ij} + \log w_2)^{-n_1+1} - (\delta - s_{ij} + \log w_1)^{-n_1+1}]}{\sum_{j=0}^l \sum_{i=0}^r \frac{h_1(j) h_2(i)}{(\delta - s_{ij})^{n_1-1}}} \right] (I_{3.1} - I_{3.2}) \\
&\quad - \text{MSq}_2 \left[ \frac{\sum_{j=0}^l \sum_{i=0}^r h_1(j) h_2(i) [(\delta - s_{ij} + \log L)^{-n_1+1} - (\delta - s_{ij} + \log w_2)^{-n_1+1}]}{\sum_{j=0}^l \sum_{i=0}^r \frac{h_1(j) h_2(i)}{(\delta - s_{ij})^{n_1-1}}} \right] (I_{3.3} \dots (5.5)
\end{aligned}$$

where

$$I_{3.1} = q_1 \left[ \frac{\sum_{j=0}^l \sum_{i=0}^r h_1(j) h_2(i) [(\delta - s_{ij} + \log w_2)^{-n_1+1} - (\delta - s_{ij} + \log w_1)^{-n_1+1}]}{\sum_{j=0}^l \sum_{i=0}^r \frac{h_1(j) h_2(i)}{(\delta - s_{ij})^{n_1-1}}} \right]$$

$$I_{3.2} = IA_{3.2} - IB_{3.2}$$

$$IA_{3.2} = \frac{q_1 - q_2}{w_2 - w_1} \left[ \frac{(n_1 - 1) \sum_{j=0}^l \sum_{i=0}^r h_1(j) h_2(i) I_{12}}{\sum_{j=0}^l \sum_{i=0}^r \frac{h_1(j) h_2(i)}{(\delta - s_{ij})^{n_1 - 1}}} \right]$$

$$IB_{3.2} = \frac{q_1 - q_2}{w_2 - w_1} \left[ W_1 \frac{\sum_{j=0}^l \sum_{i=0}^r h_1(j) h_2(i) [(\delta - s_{ij} + \log w_2)^{-n_1 + 1} - (\delta - s_{ij} + \log w_1)^{-n_1 + 1}]}{\sum_{j=0}^l \sum_{i=0}^r \frac{h_1(j) h_2(i)}{(\delta - s_{ij})^{n_1 - 1}}} \right]$$

$$I_{3.3} = \frac{1}{L - w_2} \int_{w_2}^L f(t|x) dt$$

$$= \frac{L}{L - w_2} [F(L|x) - F(w_2|x)]$$

$$= \frac{L}{L - w_2} \left[ \frac{\sum_{j=0}^l \sum_{i=0}^r h_1(j) h_2(i) [(\delta - s_{ij} + \log L)^{-n_1 + 1} - (\delta - s_{ij} + \log w_2)^{-n_1 + 1}]}{\sum_{j=0}^l \sum_{i=0}^r \frac{h_1(j) h_2(i)}{(\delta - s_{ij})^{n_1 - 1}}} \right]$$

$$I_{3.4} = \frac{1}{L - w_2} \int_{w_2}^L tf(t|x) dt$$

$$= \left( \frac{1}{L - w_2} \right) \frac{(n_1 - 1) \sum_{j=0}^l \sum_{i=0}^r h_1(j) h_2(i) I_{2L}}{\sum_{j=0}^l \sum_{i=0}^r \frac{h_1(j) h_2(i)}{(\delta - s_{ij})^{n_1 - 1}}}$$

where,

$$I_{2L} = \int_{w_2}^L (\delta - s_{ij} + \log t)^{-n_1} dt$$

after some mathematical manipulation we get the expected utility function from(5.2).

Thus the optimal warranty( $w_1^*, w_2^*$ ) is obtained by solving the optimization problem

$$(w_1^*, w_2^*) = \arg \left( \max_{w_1 \leq w_2 \in R^+} E(U(T, w_1, w_2)) \right) \quad ..(5.6)$$

where  $R^+$  denotes the set of positive real numbers

This is difficult to solve analytically but by preparing a computer program or using the available software it can be solved.

## 6. Numerical example

Let us assume the selling price of this product as  $S=200$  and its production cost is fixed as 125 by the manufacturer so that the profit per product becomes  $A_1 = 75$ . We further assume that the manufacturer fixed the proportions of loss from consumer dissatisfaction as  $q_1 = 0.2$  and  $q_2 = 0.1$ . The following data is generated from the Pareto distribution by taking  $\theta = 2.5$ :

1.019332, 1.140674, 1.165424, 1.183377, 1.212933, 1.325606, 1.423381, 1.426641, 1.52754, 1.552468, 1.69869, 1.831647, 2.121587, 2.387227, 2.640563

From the above data we consider the following types of multiply type-II censored data.

As per our notations we have  $n=15, r=3, k=3, l=2, m=1$ .

-, -, -, 1.183377, 1.212933, 1.325606, -, -, 1.52754, 1.552468, 1.69869, 1.831647, 2.121587, 2.387227.

Manufacturers also assume that the consumer satisfies the product if its life time is at least  $L$  which is the median of the posterior predictive distribution. The standard warranty under the FRW policy is set as 10<sup>th</sup> percentile of the posterior predictive distribution which is denoted by  $t_w$ . Suppose that the manufacturer wishes to set the percentage of benefit remains to be 0.8 (80%) under combined policy, then putting this value in the equation (4.3) we get the value of  $A_2$ . The values of  $L$  and  $t_w$  are shown in Table-1 to Table-5 for different values of  $\delta$  and  $\nu$ .

Based on the above assumptions the optimal warranty length and maximum value of expected utility function under FRW, PRW and combined policy are calculated and the results are shown in the Table-1 to Table-5.

## 7. Simulation study

In this section we have carried out a simulation study considering the two values of the parameter of Pareto life time model as  $\theta = 2.5$  and 12.5. Also simulation is

done 1000 times and the average values of warranty length and maximum value of expected utility function are calculated along with their standard errors in case of all the three policies. The results are shown in the following Tables.

Table-6 to Table-10 contain optimum warranty length and expected utility function with their standard errors for  $\theta=2.5$  and different values of prior parameter  $\delta$  and  $\nu$  under FRW, PRW and combined policy (FRW, PRW both). The above things are obtained in the Table-11 to Table-15 for  $\theta=12.5$ .

### **Conclusion**

In today's market product warranty plays an increasingly important role in both consumer and commercial transactions. For manufacturer it is important to decide the appropriate warranty length and appropriate warranty policy. We have provided an approach to the manufacturers to determine optimal warranty length and warranty policy based on multiply type-II censored data using Bayesian method.

From the Table - 1 to Table - 5 we observed that, for the given real data combined policy gives maximum utility followed by PRW and then by FRW for any choice of prior parameter  $\delta$  and  $\nu$ . For any fixed value of prior parameter,  $\delta$ , as  $\nu$  increases, maximum utility decreases in all the type of policies and for keeping  $\nu$  fixed, as  $\delta$  increases, maximum utility more or less remains stable. Thus maximum utility has more effect of prior parameter  $\nu$  compare to the parameter  $\delta$ .

Also from the Table - 6 and Table - 15 we observed that combined policy gives maximum utility followed by PRW and then by FRW for any choice of prior parameters. For any fixed value of prior parameter,  $\delta$ , as  $\nu$  increases, maximum utility decreases in all the type of policies and for fixed  $\nu$  as  $\delta$  increases, the value of maximum utility fluctuates.

### **Acknowledgments**

Authors are thankful to the honorable referee for making suggestions and also grateful to the chief editor for help on this work.

## References

- [1] T. Scitovszky, Some consequence of the habit of judging quality by price, *Review of economic studies*, 12, 100, **1945**.
- [2] W. R. Blischke, D. N. P. Murthy, "Warranty Cost Analysis", Marcel Dekker, **1993**.
- [3] N. D. Singpurwalla, S. P. Wilson, Failure models indexed by two scales, *Advances in Applied Probability*, .30, 1058, **1998**.
- [4] Y. S. Huang, C. H. Hsieh, J. W. Ho, Decisions on an optimal life test sampling plan with warranty considerations, *IEEE Trans. Reliab.*, 57(4), 643, **2008**.
- [5] S.J., Wu, S.R. Huang, Optimal Warranty Length for a Rayleigh Distributed Product with Progressive Censoring, *IEEE Trans. on Reliab.*, 59, 661, **2010**.
- [6] C. C. Wu, P. C. Lin, C. Y. Chou, Determination of price and warranty length for a normal lifetime distributed product, *Int. J. of Production Economics*, 102, 95, **2006**.
- [7] A. C. Cohen, Progressively censored samples in life testing, *Technometrics*, 5, 327, **1963**.
- [8] N. R. Mann, Best linear invariant estimation for Weibull Parameters under progressive censoring, *Technometrics*, 1(13), 521, **1971**.
- [9] R. Viveros, N. Balakrishnan, Interval estimation of parameters of life from progressively censored data, *Technometrics*, vol.36, pp.84-91, **1994**.
- [10] E. Gouno, A. Sen, N. Balakrishnan, Optimal step-stress test under progressive Type-I censoring. *IEEE Trans. Reliab.*, 53(3), 388, **2004**.
- [11] N. W. Patel, M. N. Patel, Progressively type-II censored samples from geometric life time model, *Journal of probab. and Statist. Sci.*, 5(1), 81, **2007**.
- [12] K. A. Gajjar, M. N. Patel, Estimation for a mixture of exponential distributions based on progressively type-II censored sample, *Int. J. of Agri. Stat. Sci.*, 4(1), 169, **2008**.
- [13] R. Aggarwala, A. Childs, Conditional inference for the parameters of Pareto distribution when observed samples are progressively censored, In "Advances in stochastic Simulation Methods" (eds: Balakrishnan. N, Meals V.B and Ermakov, S. M., Birkhauser), Boston, **1999**.
- [14] B. C. Arnold, Pareto distributions, In: *Statistical distributions in scientific work*, International Publishing House, Burtonsville, MD, **1983**.
- [15] D. S. Chareti, A. H. Morre, J. W. Cotman, A comparison of estimation techniques for the three parameters Pareto distribution, *Comm. in Statist.-Compu. and Simu.*, 17(4), 1395, **1988**.
- [16] A. M. Hossain, W. J. Zimmer, Comparisons of methods of estimation for a Pareto distribution of the first kind, *Comm. in Statist.- Theo. and Metho.*, 29(4), 859, **2000**.

- [17] M. A.W. Mahmmd, A. A. Soliman, A. H. Ahd. Ellah R. M. El-Sageer, Bayesian estimation using MCMC approach based on progressive first failure censoring from generalized Pareto distribution, *American J. of Theor. and Applied Statis.*, 2(5), 128, **2013**.
- [18] C. K. Podder, M. K. Roy, K. J. Bhuiyan, A. Karim, Minimax estimation of the parameter of the Pareto distribution under quadratic and MLINEX loss functions, *Pakistan J. of Statis.*, 20(1), 137, **2004**.
- [19] J. B. Shah, M. N. Patel, Estimator of parameter in a Pareto distribution from multiply type-II censored data, *Int. J. of Agri. Stat. Sci.*, 3( 2), 581, **2007**.
- [20] S. K. Upadhyay, U. Singh, V. Shastri, Estimation of Exponential parameters under multiply Type-II censoring, *Journal of commu. Statist.*, 25(3),801, **1996**.
- [21] N. Balakrishnan, On the maximum likelihood estimation of the parameters of exponential distribution based on multiply-II censored sample, *Journal of Applied Statistics*, 17, 55,**1990**.
- [22] K. Balasubramanian, N. Balakrishnan, Estimation for one and two parameter exponential distribution under multiply-II censoring, *Statistische Hefte*, 33, 203,**1992**.
- [23] U. Singh, A. Kumar, Bayesian Estimation of the Exponential Parameter under a Multiply Type-II Censoring Scheme, *Austrian J. of Stat.*, 36(3), 227, **2007**.
- [24] J. B. Shah, M. N. Patel, Bayes Estimation under asymmetric loss functions Multiply type II censored Rayleigh data, *Journal of Indian Stat. Asso.*, vol. 46(1), pp. 67-78, **2008**.
- [25] J. G. Patankar, A. Mitra, W. R. Blischke, D. N. P. Murthy, "Product Warranty Handbook", Marcel Dekker, **1996**.
- [26] C. A. Kelly, W. R. Blischke, D. N. P. Murthy, "Product Warranty Handbook". Marcel Dekker,**1996**.

### Tables

**Table 1. Values of L and  $t_w$ ,  $W_1^*$ ,  $W_2^*$  and MU under fixed value of  $\delta$  and different values of  $\nu$ .**

$\delta$	$\nu$	Policy	L	$t_w$	$W_1^*$	$W_2^*$	MU
5	5	FRW	2.719400	1.1601999	1.21499	-	50.142085
		PRW			-	1.6359999	58.823747
		MIX			1.09599	1.2369999	67.083957
	10	FRW	2.197100	1.124499	1.13999	-	50.051808
		PRW			-	1.4689999	57.892106
		MIX			1.06499	1.1589999	67.031533
	15	FRW	1.912299	1.1016999	1.10099	-	50.044583
		PRW			-	1.3659999	57.259553
		MIX			1.047	1.1159999	67.027256
	20	FRW	1.734499	1.0858999	1.07699	-	50.031735
		PRW			-	1.2979999	56.807513
		MIX			1.036	1.0899999	67.026054
	25	FRW	1.613599	1.0742999	1.06199	-	50.024104
		PRW			-	1.248999	56.470987
		MIX			1.029	1.0729999	67.016630

**Table 2. Values of L and  $t_w$ ,  $W_1^*$ ,  $W_2^*$  and MU under fixed value of  $\delta$  and different values of  $\nu$ .**

$\delta$	$\nu$	Policy	L	$t_w$	$W_1^*$	$W_2^*$	MU
10	5	FRW	3.277600	1.192799	1.29899	-	50.359543
		PRW			-	1.7909999	59.591841
		MIX			1.12799	1.3199999	67.090656
	10	FRW	2.546300	1.149499	1.19099	-	50.099408
		PRW			-	1.5839999	58.546317
		MIX			1.08599	1.2119999	67.092667
	15	FRW	2.160400	1.1218999	1.13499	-	50.055672
		PRW			-	1.4569999	57.820556
		MIX			1.06299	1.1539999	67.089308
	20	FRW	1.924699	1.1028999	1.10199	-	50.04158
		PRW			-	1.3719999	57.292507
		MIX			1.048	1.1189999	67.074514
	25	FRW	1.766799	1.0889999	1.08099	-	50.037529
		PRW			-	1.3109999	56.895081
		MIX			1.039	1.0959999	67.047922

**Table 3. Values of L and  $t_w$ ,  $W_1^*$ ,  $W_2^*$  and MU under fixed value of  $\delta$  and different values of  $\nu$ .**

$\delta$	$\nu$	Policy	L	$t_w$	$W_1^*$	$W_2^*$	MU
15	5	FRW	3.948800	1.226299	1.39799	-	50.690741
		PRW			-	1.9519999	60.30250
		MIX			1.16299	1.414999	67.09416
	10	FRW	2.949900	1.174899	1.25099	-	50.228970
		PRW			-	1.7049999	59.172026
		MIX			1.10999	1.2729999	67.083731
	15	FRW	2.439800	1.1424999	1.17499	-	50.081123
		PRW			-	1.5509999	58.363926
		MIX			1.07999	1.196999	67.071978
	20	FRW	2.135000	1.1200999	1.13199	-	50.05843
		PRW			-	1.4479999	57.769642
		MIX			1.06099	1.1499999	67.064765
	25	FRW	1.933899	1.1037999	1.10399	-	50.043673
		PRW			-	1.3749999	57.316563
		MIX			1.049	1.119999	67.052355

**Table 4. Values of  $L$  and  $t_w$ ,  $W_1^*$ ,  $W_2^*$  and MU under fixed value of  $\delta$  and different values of  $v$ .**

$\delta$	$v$	Policy	L	$t_w$	$W_1^*$	$W_2^*$	MU
20	5	FRW	4.756200	1.2606999	1.51499	-	51.120455
		PRW			-	2.1169999	60.955419
		MIX			1.19999	1.5209999	67.207231
	10	FRW	3.416600	1.2008999	1.32099	-	50.432553
		PRW			-	1.8289999	59.762707
		MIX			1.13599	1.3419999	67.099718
	15	FRW	2.754700	1.1633999	1.22199	-	50.162539
		PRW			-	1.6489999	58.888675
		MIX			1.09899	1.2449999	67.085310
	20	FRW	2.367700	1.1375999	1.16499	-	50.072188
		PRW			-	1.5279999	58.234409
		MIX			1.07599	1.1859999	67.079943
	25	FRW	2.116400	1.1187999	1.12899	-	50.059963
		PRW			-	1.4419999	57.731158
		MIX			1.05999	1.1479999	67.068482

**Table 5. Values of L and  $t_w$ ,  $W_1^*$ ,  $W_2^*$  and MU under fixed value of  $\delta$  and different values of  $\nu$ .**

$\delta$	$\nu$	Policy	L	$t_w$	$W_1^*$	$W_2^*$	MU
25	5	FRW	5.727800	1.2958999	1.64699	-	51.630296
		PRW			-	2.284999	61.553716
		MIX			1.23899	1.6379999	67.30315
	10	FRW	3.956600	1.2274999	1.40199	-	50.704339
		PRW			-	1.955999	60.317131
		MIX			1.16399	1.4179999	67.137219
	15	FRW	3.109700	1.1845999	1.27599	-	50.298229
		PRW			-	1.7499999	59.392547
		MIX			1.11899	1.2969999	67.087862
	20	FRW	2.625400	1.1552999	1.20299	-	50.127057
		PRW			-	1.6099999	58.686678
		MIX			1.09099	1.224999	67.080577
	25	FRW	2.315700	1.133999	1.15799	-	50.067108
		PRW			-	1.510999	58.137319
		MIX			1.07199	1.177999	67.076366

**Table 6. Values of  $W_1^*$ ,  $W_2^*$ , MU, Std  $W_1^*$ , Std  $W_2^*$  and StdMU under fixed value of  $\delta$  and different values of  $v$ .**

$\delta$	$v$	Policy	$W_1^*$	$W_2^*$	MU	Std $W_1^*$	Std $W_2^*$	StdMU
5	5	FRW	1.06429	-	45.151703	0.363585	-	15.05098
		PRW	-	1.34169	52.149674	-	0.476331	17.40994
		MIX	0.96749	1.06749	60.419687	0.323612	0.362098	20.14000
	10	FRW	1.00299	-	45.110040	0.337630	-	15.03697
		PRW	-	1.21679	51.401973	-	0.422181	17.15128
		MIX	0.94409	1.00909	60.404112	0.315166	0.338943	20.13156
	15	FRW	0.97279	-	45.108394	0.325824	-	15.03343
		PRW	-	1.14349	50.919725	-	0.391627	16.98478
		MIX	0.93189	0.97919	60.391518	0.310863	0.327672	20.12404
	20	FRW	0.95529	-	45.097360	0.319287	-	15.0452
		PRW	-	1.09599	50.593226	-	0.372374	16.87262
		MIX	0.92449	0.96139	60.389191	0.308295	0.321194	20.10325
	25	FRW	0.94419	-	45.084594	0.315261	-	15.03900
		PRW	-	1.06309	50.349282	-	0.359341	16.78910
		MIX	0.91979	0.94989	60.376847	0.306679	0.317093	20.11913

**Table 7. Values of  $W_1^*$ ,  $W_2^*$ , MU, Std  $W_1^*$ , Std  $W_2^*$  and StdMU under value of  $\delta$  and different values of  $\nu$ .**

$\delta$	$\nu$	Policy	$W_1^*$	$W_2^*$	MU	Std $W_1^*$	Std $W_2^*$	Std MU
10	5	FRW	1.13949	-	45.28382	0.392806	-	15.09671
		PRW	-	1.48809	52.95434	-	0.525973	17.67514
		MIX	0.99619	1.14069	60.39026	0.333570	0.388854	20.13010
	10	FRW	1.04709	-	45.09916	0.353856	-	15.03319
		PRW	-	1.32169	52.05373	-	0.458110	17.36752
		MIX	0.96259	1.05449	60.38145	0.321496	0.355018	20.14056
	15	FRW	1.00209	-	45.09096	0.336250	-	15.03050
		PRW	-	1.22389	51.46250	-	0.419175	17.16551
		MIX	0.94469	1.01029	60.37585	0.315223	0.338539	20.15874
	20	FRW	0.96819	-	45.05907	0.323685	-	15.05340
		PRW	-	1.18499	51.21213	-	0.403728	17.07999
		MIX	0.93399	0.98439	60.33164	0.311506	0.329112	20.17734
	25	FRW	0.96049	-	45.04512	0.320878	-	15.06548
		PRW	-	1.11639	50.74350	-	0.377584	16.92066
		MIX	0.92709	0.96759	60.31180	0.309141	0.323135	20.19406

**Table 8. Values of  $W_1^*$ ,  $W_2^*$ , MU, Std  $W_1^*$ , Std  $W_2^*$  and StdMU under fixed value of  $\delta$  and different values of  $\nu$ .**

$\delta$	$\nu$	Policy	$W_1^*$	$W_2^*$	MU	Std $W_1^*$	Std $W_2^*$	StdMU
15	5	FRW	1.23199	-	45.55691	0.42855	-	15.19088
		PRW	-	1.64279	53.71080	-	0.577415	17.92380
		MIX	1.02879	1.22719	60.40548	0.34473	0.420038	20.13520
	10	FRW	1.10039	-	45.17531	0.37349	-	15.05907
		PRW	-	1.43329	52.68856	-	0.495765	17.57766
		MIX	0.98369	1.10769	60.38989	0.32871	0.373859	20.12998
	15	FRW	1.03719	-	45.07966	0.34874	-	15.02659
		PRW	-	1.30959	51.99423	-	0.448234	17.34216
		MIX	0.95959	1.04679	60.37345	0.32028	0.351221	20.14121
	20	FRW	1.00159	-	45.06247	0.33546	-	15.02758
		PRW	-	1.22919	51.50164	-	0.417783	17.17534
		MIX	0.94509	1.01119	60.36158	0.31526	0.338326	20.15727
	25	FRW	0.97949	-	45.05542	0.32744	-	15.03869
		PRW	-	1.17339	51.13628	-	0.396927	17.05150
		MIX	0.93549	0.98819	60.35990	0.31197	0.330159	20.17338

**Table 9. Values of  $W_1^*$ ,  $W_2^*$ , MU, Std  $W_1^*$ , Std  $W_2^*$  and StdMU under fixed value of  $\delta$  and different values of  $\nu$ .**

$\delta$	$\nu$	Policy	$W_1^*$	$W_2^*$	MU	Std $W_1^*$	Std $W_2^*$	StdMU
20	5	FRW	1.34259	-	45.94179	0.470473	-	15.32309
		PRW	-	1.80399	54.40956	-	0.630583	18.15309
		MIX	1.06469	1.32719	60.46174	0.356953	0.455543	20.15404
	10	FRW	1.16409	-	45.33235	0.396913	-	15.11255
		PRW	-	1.55039	53.29281	-	0.534934	17.77744
		MIX	1.00759	1.16949	60.38433	0.336835	0.395562	20.12811
	15	FRW	1.07849	-	45.12493	0.363506	-	15.04189
		PRW	-	1.39959	52.51633	-	0.478535	17.51550
		MIX	0.97629	1.08859	60.38075	0.325933	0.365705	20.13026
	20	FRW	1.03079	-	45.07065	0.345683	-	15.02357
		PRW	-	1.30129	51.95182	-	0.442098	17.32500
		MIX	0.95749	1.04139	60.37465	0.319456	0.348730	20.14159
	25	FRW	1.00139	-	45.07064	-	0.334988	15.02604
		PRW	-	1.23289	51.53630	-	0.417033	17.18480
		MIX	0.94529	1.01179	60.36786	0.315270	0.338205	20.15601

**Table 10. Values of  $W_1^*$ ,  $W_2^*$ , MU, Std  $W_1^*$ , Std  $W_2^*$  and StdMU under fixed value of  $\delta$  and different values of  $\nu$ .**

$\delta$	$\nu$	Policy	$W_1^*$	$W_2^*$	MU	Std $W_1^*$	Std $W_2^*$	StdMU
25	5	FRW	1.4702	-	46.415623	0.517417	-	15.48469
		PRW	-	1.97029	55.044745	-	0.685150	18.36177
		MIX	1.1028	1.43959	60.543675	0.369836	0.494873	20.18145
	10	FRW	1.2384	-	45.566884	0.424028	-	15.19244
		PRW	-	1.67149	53.865160	-	0.575145	17.96653
		MIX	1.0334	1.23929	60.407819	0.345622	0.419969	20.13597
	15	FRW	1.1261	-	45.225867	0.380526	-	15.07605
		PRW	-	1.49319	53.016096	-	0.509821	17.68133
		MIX	0.9949	1.13599	60.379444	0.332268	0.382117	20.12648
	20	FRW	1.0642	-	45.097300	0.357402	-	15.03254
		PRW	-	1.37679	52.392567	-	0.467457	17.47143
		MIX	0.9713	1.07619	60.364694	0.324135	0.360648	20.13158
	25	FRW	1.0261	-	45.059548	0.343586	-	15.01986
		PRW	-	1.29559	51.923593	-	0.438130	17.31368
		MIX	0.9560	1.03809	60.359701	0.318911	0.347185	20.14326

**Table 11. Values of  $W_1^*$ ,  $W_2^*$ , MU, Std  $W_1^*$ , Std  $W_2^*$  and StdMU under fixed value of  $\delta$  and different values of  $\nu$ .**

$\delta$	$\nu$	Policy	$W_1^*$	$W_2^*$	MU	Std $W_1^*$	Std $W_2^*$	StdMU
5	5	FRW	0.93369	-	45.451807	0.31131	-	15.11747
		PRW	-	1.03909	50.179587	-	0.34729	16.72769
		MIX	0.91539	0.93959	60.791721	0.30514	0.31327	20.23061
	10	FRW	0.92339	-	45.380970	0.30783	-	15.16048
		PRW	-	1.00039	49.875158	-	0.33396	16.62571
		MIX	0.911	0.92839	60.767713	0.30367	0.30949	20.25592
	15	FRW	0.91769	-	45.372282	0.30591	-	15.19088
		PRW	-	0.97789	49.696735	-	0.32626	16.56597
		MIX	0.9093	0.92279	60.751597	0.30310	0.30760	20.27054
	20	FRW	0.91419	-	45.363038	0.30474	-	15.21022
		PRW	-	0.96309	49.571583	-	0.32122	16.52414
		MIX	0.909	0.92	60.723963	0.303	0.30667	20.27465
	25	FRW	0.91179	-	45.350232	0.30394	-	15.22681
		PRW	-	0.95279	49.489879	-	0.31773	16.49680
		MIX	0.909	0.9187	60.714525	0.303	0.30623	20.26490

**Table 12. Values of  $W_1^*$ ,  $W_2^*$ , MU, Std  $W_1^*$ , Std  $W_2^*$  and StdMU under fixed value of  $\delta$  and different values of  $\nu$ .**

$\delta$	$\nu$	Policy	$W_1^*$	$W_2^*$	MU	Std $W_1^*$	Std $W_2^*$	StdMU
10	5	FRW	0.96869	-	45.220020	0.323062	-	15.04005
		PRW	-	1.15759	51.040941	-	0.386986	17.01486
		MIX	0.93179	0.97929	60.631027	0.310625	0.326569	20.17702
	10	FRW	0.94609	-	45.219570	0.315431	-	15.08327
		PRW	-	1.08519	50.528729	-	0.362338	16.84362
		MIX	0.92129	0.95099	60.623054	0.307110	0.318091	20.20770
	15	FRW	0.93389	-	45.200705	0.311332	-	15.11697
		PRW	-	1.04279	50.208084	-	0.347970	16.73646
		MIX	0.91559	0.94039	60.612907	0.305204	0.313495	20.23098
	20	FRW	0.92569	-	45.198310	0.308583	-	15.14949
		PRW	-	1.01949	50.023986	-	0.340109	16.67501
		MIX	0.9123	0.93209	60.603676	0.304103	0.310718	20.24790
25	FRW	0.92179	-	45.189937	0.307279	-	15.16670	
	PRW	-	0.99619	49.843419	-	0.332236	16.61467	
	MIX	0.9103	0.92679	60.592725	0.303434	0.308944	20.26091	

**Table 13. Values of  $W_1^*$ ,  $W_2^*$ , MU, Std  $W_1^*$ , Std  $W_2^*$  and StdMU under fixed value of  $\delta$  and different values of  $\nu$ .**

$\delta$	$\nu$	Policy	$W_1^*$	$W_2^*$	MU	Std $W_1^*$	Std $W_2^*$	StdMU
15	5	FRW	1.06659	-	45.11854	0.356118	-	15.02287
		PRW	-	1.40279	52.55410	-	0.469439	17.51953
		MIX	0.97389	1.08259	60.38059	0.324710	0.361303	20.12686
	10	FRW	0.97559	-	45.10922	0.325307	-	15.03309
		PRW	-	1.18039	51.19817	-	0.394134	17.06675
		MIX	0.93509	0.98719	60.37262	0.311715	0.329154	20.17088
	15	FRW	0.95449	-	45.09308	0.318219	-	15.06440
		PRW	-	1.11589	50.74967	-	0.372378	16.91704
		MIX	0.92559	0.96419	60.36551	0.308542	0.321446	20.19518
	20	FRW	0.94209	-	45.07822	0.314061	-	15.09278
		PRW	-	1.07389	50.44675	-	0.358246	16.81589
		MIX	0.91989	0.95009	60.35639	0.306638	0.316728	20.21547
25	FRW	0.93359	-	45.06054	0.311218	-	15.12021	
	PRW	-	1.04819	50.25306	-	0.349626	16.75128	
	MIX	0.91589	0.94089	60.34982	0.305303	0.313652	20.22994	

**Table 14. Values of  $W_1^*$ ,  $W_2^*$ , MU, Std  $W_1^*$ , Std  $W_2^*$  and StdMU under fixed value of  $\delta$  and different values of  $\nu$ .**

$\delta$	$\nu$	Policy	$W_1^*$	$W_2^*$	MU	Std $W_1^*$	Std $W_2^*$	StdMU
20	5	FRW	1.08089	-	45.09397	0.360729	-	15.03136
		PRW	-	1.43569	52.73450	-	0.479813	17.57915
		MIX	0.97999	1.09789	60.47575	0.326719	0.366274	20.12525
	10	FRW	1.01359	-	45.08833	0.338024	-	15.01278
		PRW	-	1.28379	51.86105	-	0.428649	17.28770
		MIX	0.95219	1.02849	60.43369	0.317423	0.342959	20.14456
	15	FRW	0.98039	-	45.07885	0.326871	-	15.02963
		PRW	-	1.19499	51.29335	-	0.398788	17.09827
		MIX	0.93739	0.99269	60.42865	0.312476	0.330955	20.16623
	20	FRW	0.96119	-	45.05766	0.320441	-	15.05258
		PRW	-	1.13719	50.90203	-	0.379373	16.96767
		MIX	0.92869	0.97149	60.41957	0.309572	0.323867	20.18653
25	FRW	0.94859	-	45.03193	0.316224	-	15.07733	
	PRW	-	1.09739	50.61822	-	0.366015	16.87300	
	MIX	0.92299	0.95769	60.41120	0.307670	0.319254	20.20374	

**Table 15. Values of  $W_1^*$ ,  $W_2^*$ , MU, Std  $W_1^*$ , Std  $W_2^*$  and StdMU under fixed value of  $\delta$  and different value of  $\nu$ .**

$\delta$	$\nu$	Policy	$W_1^*$	$W_2^*$	MU	Std $W_1^*$	Std $W_2^*$	StdMU
25	5	FRW	1.16199	-	45.29221	0.387963	-	15.09756
		PRW	-	1.58929	53.51308	-	0.531012	17.83856
		MIX	1.01149	1.17889	60.39394	0.337238	0.393391	20.12464
	10	FRW	1.06069	-	45.26584	0.353794	-	15.02195
		PRW	-	1.39419	52.50690	-	0.465478	17.50291
		MIX	0.97219	1.07789	60.38624	0.324097	0.359472	20.12874
	15	FRW	1.01149	-	45.24036	0.337270	-	15.01345
		PRW	-	1.27939	51.83578	-	0.426948	17.27903
		MIX	0.95129	1.02629	60.37620	0.317115	0.342183	20.14540
	20	FRW	0.98349	-	45.22446	0.327888	-	15.02816
		PRW	-	1.20489	51.36459	-	0.401957	17.12184
		MIX	0.93909	0.99659	60.36161	0.313042	0.332245	20.16387
25	FRW	0.96589	-	45.14401	0.322000	-	15.04801	
	PRW	-	1.15329	51.01085	-	0.384660	17.00386	
	MIX	0.93089	0.97719	60.34249	0.310304	0.325759	20.18083	

-----

# NON-LINEAR FINITE ELEMENT ANALYSIS OF STRESS AND STRESS INTENSITY FACTOR ACROSS THE ADHESIVE THICKNESS IN COMPOSITE SINGLE-LAP JOINTS

**J. D. Rathod, K. Sheth**

Applied Mechanics and Structural Engineering Department,  
Faculty of Technology and Engineering,  
The Maharaja Sayajirao University of Baroda, Vadodara - 390001.  
E-mail : [jdrathod-appmech@msubaroda.ac.in](mailto:jdrathod-appmech@msubaroda.ac.in)  
E-mail : [krishna.sheth@gmail.com](mailto:krishna.sheth@gmail.com)

## Abstract

Inherent complexity of fiber-reinforced laminated composites poses challenges to manufacture composite structures according to their exact design specifications. Proper understanding of uncertainties in laminated structures and their effect on static responses is highly important for a reliable design of such structures. This paper focuses the static analysis of stress and stress intensity factor by introducing crack in adhesive material which is used to bond laminated FRP composites in a single lap joint in using three dimensional theory of finite element method. Ply orientation of  $0^\circ$  with multi linear isotropic material property for adhesive in laminated composites is considered for analysis. Crack is introduced in middle portion of adhesive layer in single lap joint laminated composites. Effect of increase in crack length, lap length and change of crack position on stress-strain and stress-stress intensity factor in adhesive is studied. Stress-strain response with respect to change in crack length and lap length is uncertain whereas stress intensity factor remains same by changing lap length. Bond failure between bottom adhered and adhesive layer is found when crack is located within the overlap joint whereas bond failure between upper adhered and adhesive layer likely to take place when crack is located outside the overlap joint.

**Keywords:** Stress intensity factor, overlap joint, adhered, adhesive

## 1. Introduction

A composite material is defined as a material system which consists of a mixture or a combination of two or more distinctly differing material which is insoluble in each other and differs in form or chemical composition. Fiber reinforced plastic

(FRP) materials are very successful in structural applications. They are widely used in the aerospace, automotive and marine industries. FRP materials or composites behave differently than typical metals such as steel or aluminum being different in micro structure [1,2]. A typical composite contains number of layers consisting of aligned fibers oriented at different angles held together by a resin matrix, giving high strength and stiffness in desired directions [3]. The joint can potentially become the weakest link in the structure because of the large amount of load it has to transfer. There are wide varieties of techniques to join different parts together. Two methods are most common which include mechanical fastening and adhesive bonding. Adhesive bonding of laminates has significant advantages over conventional mechanical fastening system [4]. Bonded joints are significantly more fatigue resistant than mechanically fastened one because of the absence of stress concentration at location of fasteners [5,6]. Also, joints may be lighter due to the absence of fastener assembly. It can be made stronger than the ultimate strength of many metals because of which it is most common in aircraft construction [7,8].

The stresses induced at the interfaces of the adhesive layer and adhesive play crucial role in the design of adhesively bonded joints in FRP composites [9]. Hence, these stresses are required to be analyzed most accurately and be considered in calculation. Most research papers have reported effect of change in crack length located within the joint, however, effect of location of crack in lap joint has not been paid much attention in the analysis. The objective of this paper is to study effect of increase of crack length in adhesive layer, increase of lap length in laminate and change of crack position in adhesive layer in single lap joint laminated composites on stress-strain and stress-stress intensity factor with the help of ANSYS 10 software.

## **2. Materials and Methodology**

### **Material Properties**

The material considered for the laminated composites is Graphite/Epoxy FRP. A single lap joint laminated composite comprises of two materials viz. adhered and adhesive for which material properties are considered as follow:

#### **Graphite /Epoxy FRP (adhered)**

The unidirectional layer orthotropic properties for the material are considered as:

$$\begin{aligned}
 E_{xy} &= 172.72 \text{ GPa}, & E_{yz} &= 6.909 \text{ GPa}, & E_{zx} &= 6.909 \text{ GPa} \\
 \gamma_{xy} &= 0.25, & \gamma_{yz} &= 0.25, & \gamma_{xz} &= 0.25 \\
 G_{xy} &= 3.45 \text{ GPa}, & G_{yz} &= 1.38 \text{ GPa}, & G_{xz} &= 3.45 \text{ GPa}
 \end{aligned}$$

where  $E_{xy}$ ,  $E_{yz}$ , and  $E_{zx}$  are the Young's module of the composite lamina along the material coordinates.  $G_{xy}$ ,  $G_{yz}$ , and  $G_{xz}$  are the Shear moduli and  $\gamma_{xy}$ ,  $\gamma_{yz}$ , and  $\gamma_{xz}$  are Poisson's ratio with respect to the X-Y, Y-Z, and Z-X planes, respectively.

**Epoxy (adhesive)**

A two laminated composite beams are joined by adhesive material for which properties are considered as:

Young's modulus (E) = 5.171 GPa, Poisson's Ratio ( $\gamma$ ) = 0.35

Material for adhesive layer is considered as multi linear for which stress-strain relationship is considered as indicated Fig. 1[7].

**Geometry**

A single lap joint laminated composite model is considered in which both adherents are considered to be symmetrically oriented and consisting of four layers of each orientation. Two laminated composites of length 100 mm, thickness of each layer 2 mm and width of 25 mm is considered as shown in Fig. 2. The stacking sequence of laminates is kept as  $0^0/90^0/90^0/0^0$ .

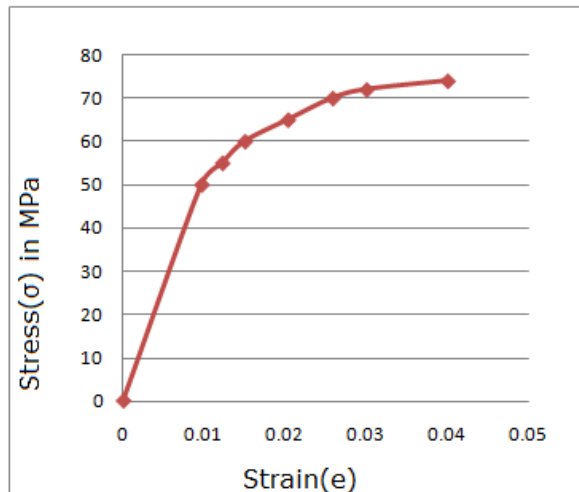


**Figure 1. Multi linear response of adhesive material**

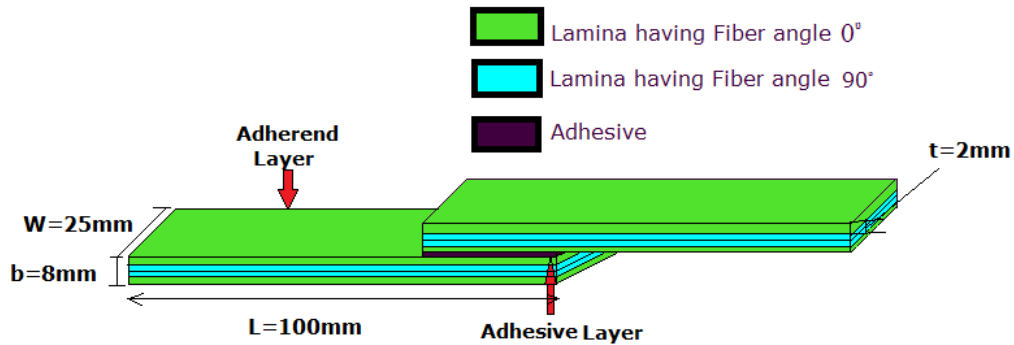


**Figure 2. Geometry of single lap joint**

Crack is introduced in adhesive layer of laminated composites as shown in Fig. 3.



**Figure 3. Geometry of introduced crack in adhesive layer**

### **Finite Element Model**

ANSYS 10.0 has been used to develop the finite element model. 20 nodes SOLID 191 3D structured element is used for adhered layer as this element is for solid laminate models only. 8 nodes SOLID 45 3D element is used for adhesive layer being isotropic material. A simple element is chosen in model to reduce the computation time. However, choice of the element over higher order element doesn't comprise the accuracy, as the choice is based on test of SOLID45 for

basic and simple problems involving ability of the element to capture transverse shear effect in deflection. Schematic representation of selected elements for adhered layer and adhesive layer to develop 3D single lap joint laminated composite model is shown in Fig. 4.

FRANC2D/L is a two dimensional, finite element based program for simulating crack propagation in layered structures. Initial mesh is generated in CASCA which is a simple pre-processor for FRANC2D/L followed by merging CASCA input file into FRANC2D using %castofranc function.

Single lap joint laminated composites are considered to be fixed at one end and free at other end. Varying twisting moment in form of load is applied at free edge. Elastic properties of adhered and adhesive materials are considered in modeling as mentioned in the material properties.

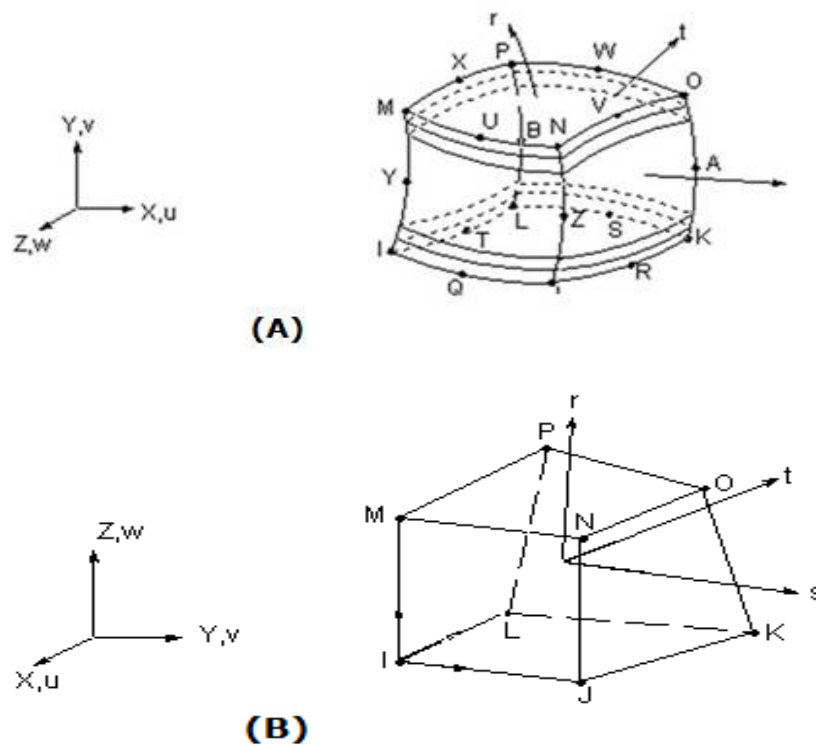


**Figure 4. Element type (A) SOLID 191 (B) SOLID 45**

Fig. 5 depicts the finite element meshing on the overlap region of the single lap joint.

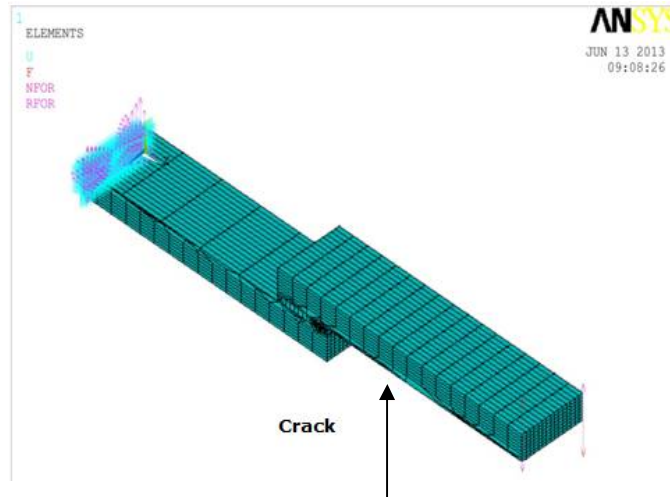


**Figure 5. Finite element meshing of single lap joint**

### **3. Results and discussion**

#### **Stress analysis around the crack**

Crack is introduced in adhesive layer and twisting moment is applied at the free end in form of load and slowly increased as a result of which crack length is increased. Points a, b, c, and d are selected around the crack in adhesive layer as shown in Fig. 6 on which the stress-strain behaviors is studied.

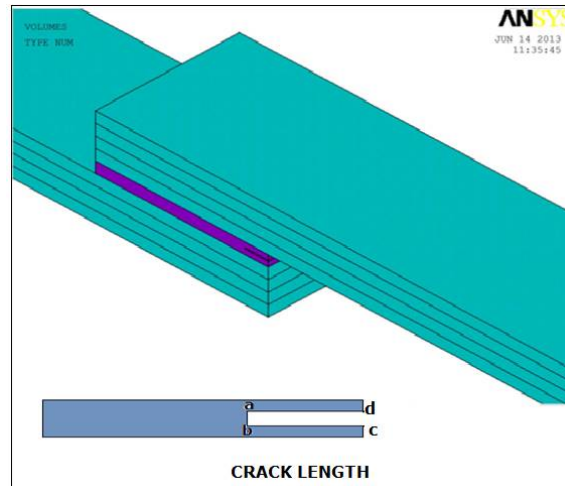


Figure 6. Crack in adhesive layer

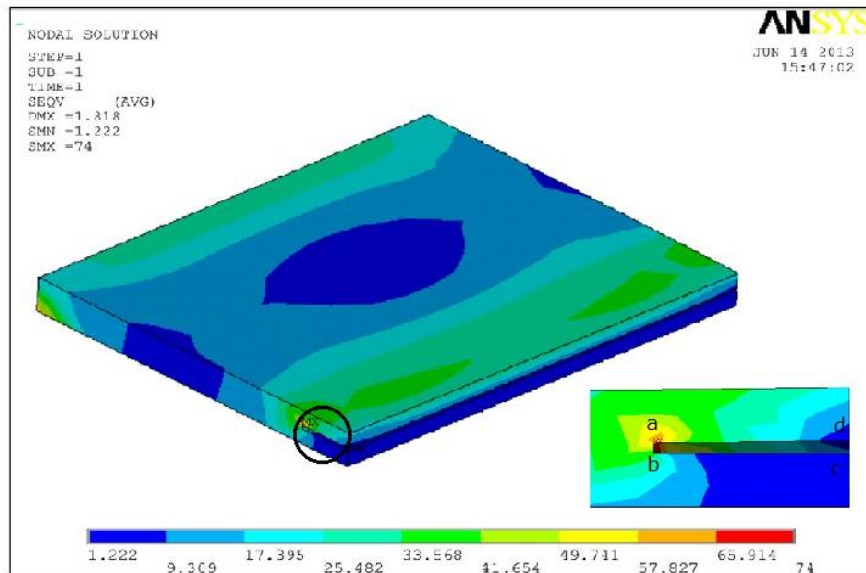


Figure 7. Von Mises stresses on adhesive layer

Stress at a point 'a' is found to be more than b, c, and d points as indicated in Table 1 which can also be verified by red colour at the point "a" depicted in Fig. 7. Blue colour at point d indicates minimum value of stress.

Relation between stress and stress intensity factor is given by the equation,

$$K = \sigma\sqrt{\pi a}$$

Where, K = stress intensity factor (MPa√mm), a = crack length (mm) and  $\sigma$  = stress (MPa)

**Table 1. Stress intensity factor at points around crack**

Points	$\sigma$ (MPa)	a (mm)	K (MPa√mm)
a	67.931	3	203.7
b	52.575	3	157.7
c	7.8314	3	23.4
d	1.911	3	5.7

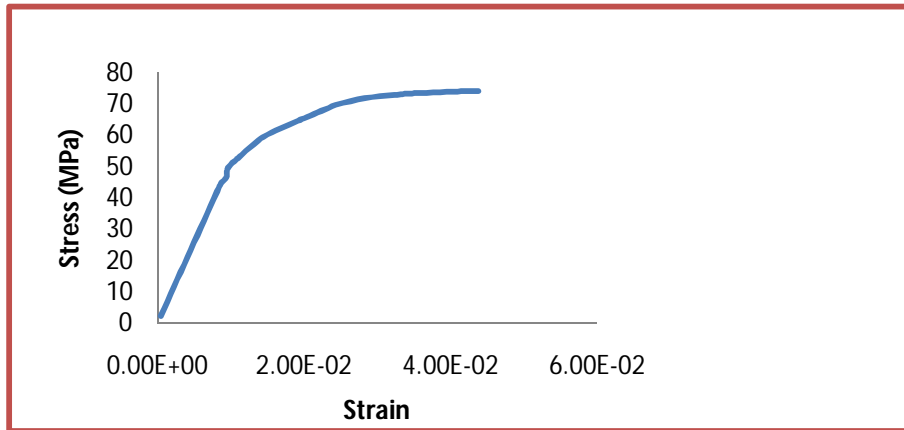
Stress intensity factor is found to be the maximum at point 'a' which indicates that crack might be propagated at point 'a'.

#### **Effect of increase in crack length on stress-strain and stress-stress intensity factor**

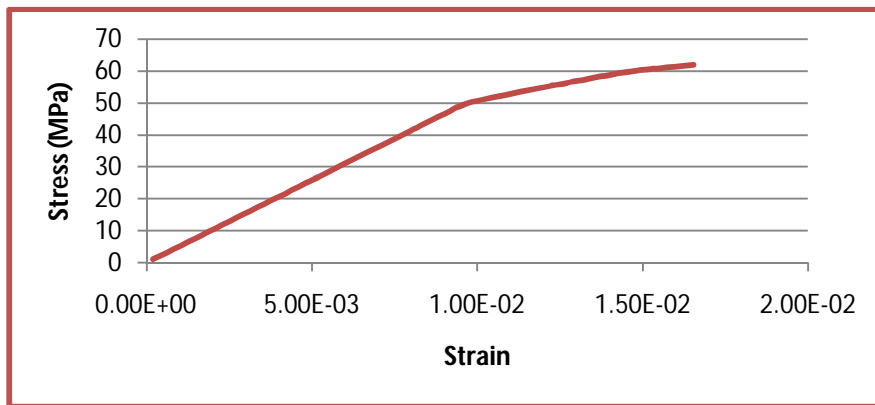
20 mm lap length is considered to join two adherents which have orthotropic property and symmetric cross ply laminates. Crack length of 3, 4, and 5 mm is considered for which effect on stress-strain and stress-stress intensity factor is studied. Twisting moment is applied in form of load at free end of edges of top adhered while the bottom adhered is considered as fixed. Point "a" is selected for study as it subjected to maximum stress.

Figs. 8 (a), (b) and (c) indicate stress v/s strain behavior at point 'a' for 3 mm, 4 mm and 5 mm crack length respectively. It can be said that stress reaches to the

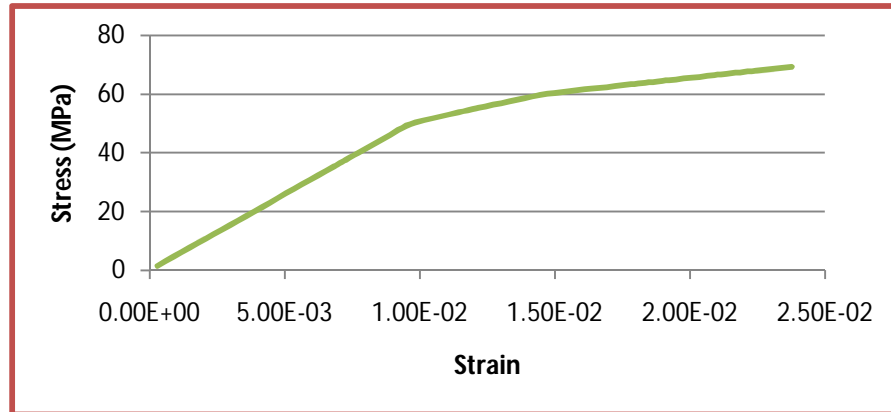
yield point for 3 mm and 5 mm crack length at the load of 670 N, whereas, stress does not reach to the yield point for 4 mm crack length.



(a) 3 mm crack length



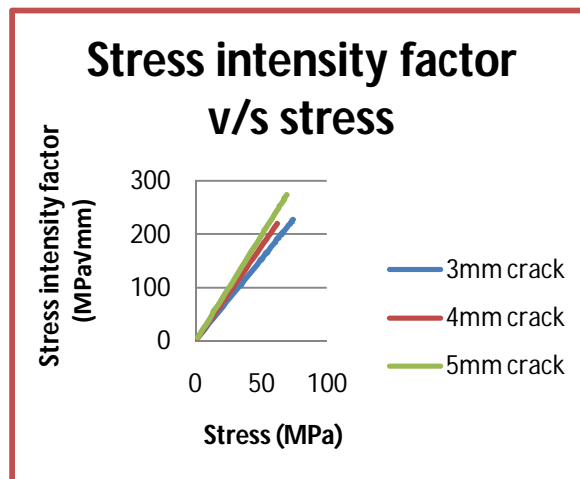
(b) 4 mm crack length



(c) 5 mm crack length

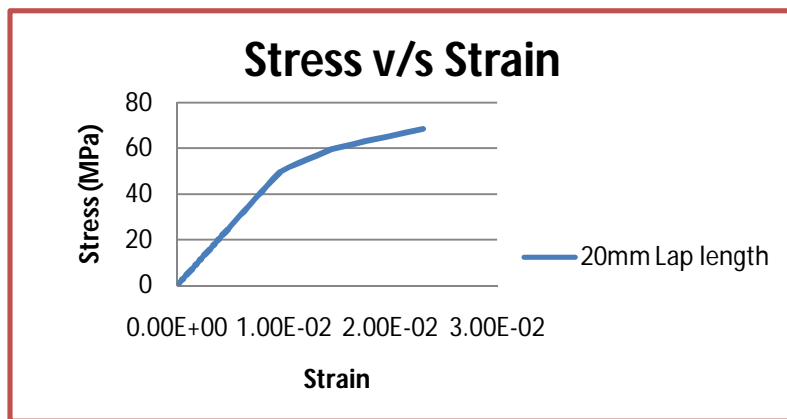
**Figure 8. Stress-strain response of crack**

Effect of increase in crack length on stress v/s stress intensity factor reveal that stress intensity factor increases with increase in stress linearly as shown in Fig. 9. Stress intensity factor for 4 mm crack length is the lowest as compared to 3 mm and 5 mm. Uncertain variation in stress intensity factor with change in crack length may be because of multi linearity applied to the adhesive layer.

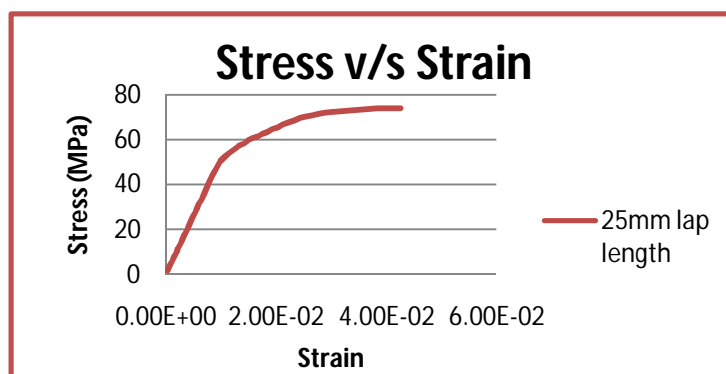
**Figure 9. Stress-Stress intensity factor response for different crack length**

**Effect of increase in lap length on stress-strain and stress-stress intensity factor**

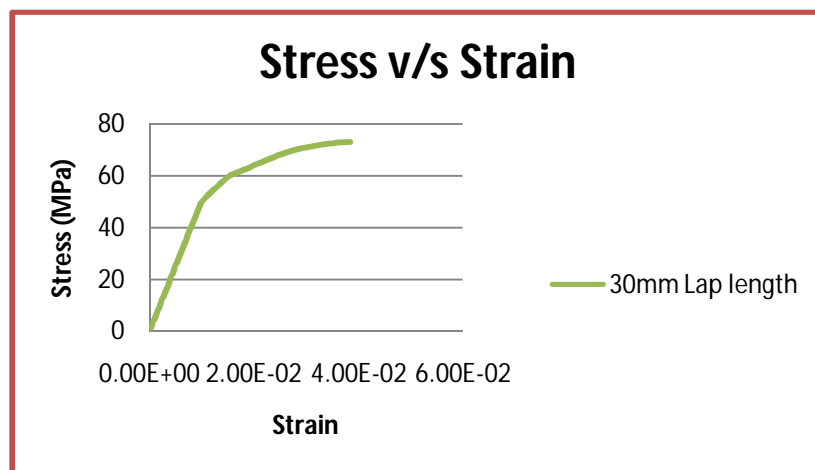
Lap lengths are considered as 20, 25 and 30 mm for which effect on stress-strain and stress-stress intensity factor is studied. Fig. 10 (a) indicates stress v/s strain response for 20 mm lap length wherein it is found that stress remains far away from yield point as compared to other two lap lengths when 820 N load is applied. Fig. 10 (b) and (c) indicate stress v/s strain at 25 mm and 30 mm lap length respectively in which stress is reached to yield point when 820 N load is applied. Thus, it can be said that due to multi linearity in adhesive layer, stress variation is observed unusual in it when lap length of adherents are increased.



(a)



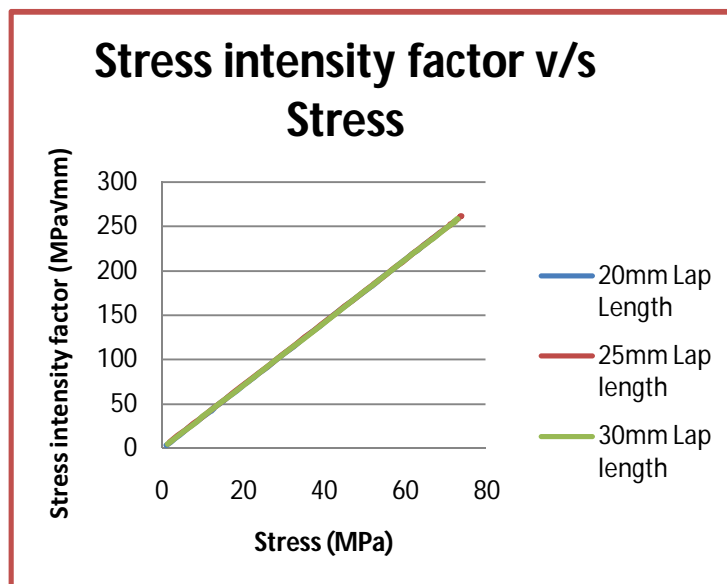
(b)



(c)

**Figure 10. Stress-strain response with change in lap length**

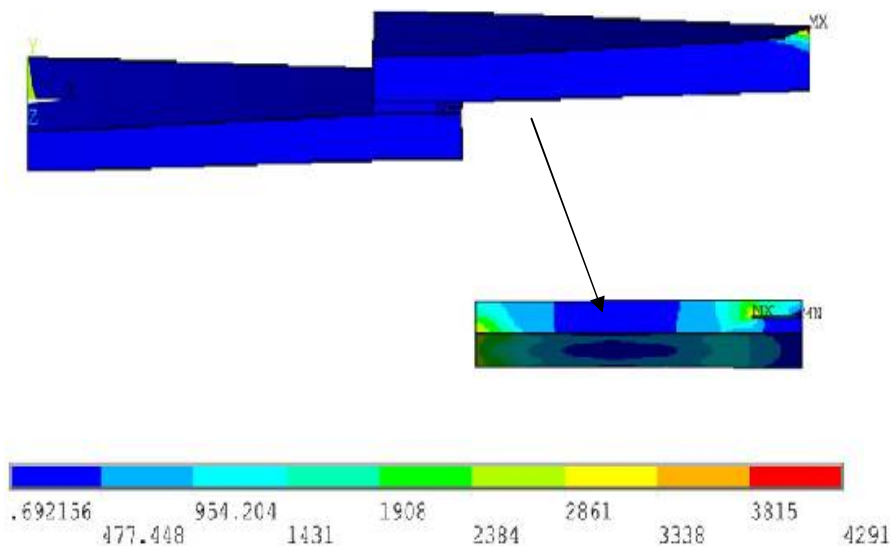
Effect of increase in lap length on stress v/s stress intensity factor indicated linear behavior as shown in Fig. 11. Stress intensity factor much depends on crack length. Therefore, there is no change in stress intensity factor of adhesive layer with increase in lap length. It is to be noted that crack length is kept constant as 3 mm for all lap lengths.

**Figure 11. Stress-stress intensity factor in adhesive for various lap lengths**

### Effect of crack location on stress-strain and stress-stress intensity factor

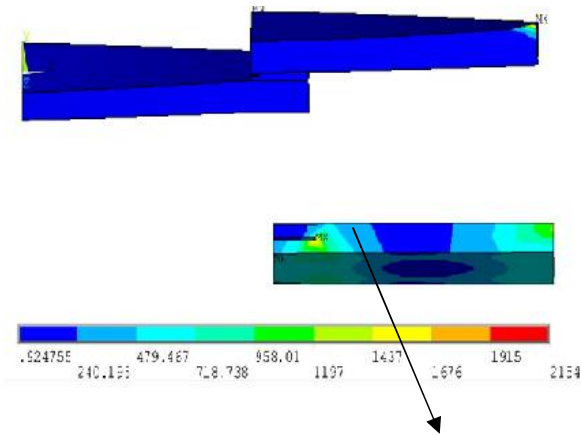
Crack length of 3 mm is provided inside and outside the overlap joint for which stress-strain and stress-stress intensity factor is studied.

It can be said from Fig. 12 that stress is the maximum at upper face of crack tip when crack is located inside the overlap joint whereas middle part of adhesive layer is subjected to minimum stress indicating very strong bond in middle. However, lower face of adhesive layer is subjected to maximum stress in a portion of adhesive wherein crack does not exist indicating bond failure between bottom adhered and adhesive layer.



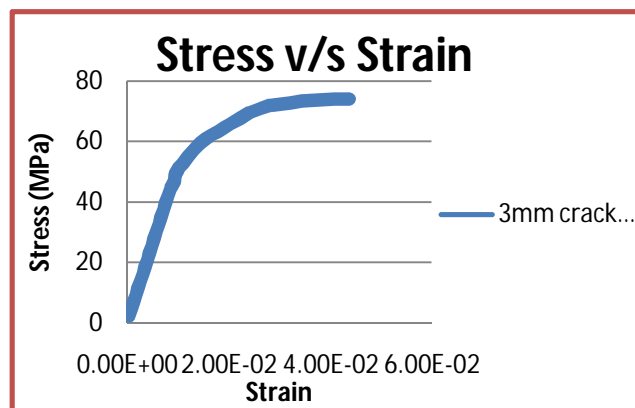
**Figure 12. Crack inside the overlap joint**

Fig. 13 depicts stresses when crack location is outside the overlap joint. It indicates that stress is the maximum at lower face of crack tip whereas middle part of adhesive layer is subjected to minimum stress indicating very strong bond in middle. Upper face of adhesive layer is subjected to the maximum stress in a portion of adhesive wherein crack does not exist indicating bond failure between top adhered and adhesive layer.



**Figure 13. Crack outside the overlap joint**

Fig. 14 depicts stress v/s strain response for 20 mm lap length with 3 mm crack inside the joint overlap. It indicates that stress is reached to yield point when 670 N load is applied. Fig. 15 depicts stress v/s strain response for 20 mm lap length with 3 mm crack outside the joint overlap. It indicates that stress is far from yield point when 670 N load is applied. Therefore, it can be said that when crack is provided outside the overlap joint, it sustains more load to reach yield point as compared to crack inside the overlap joint.



**Figure 14. Stress-strain response when crack is provided inside the overlap joint**

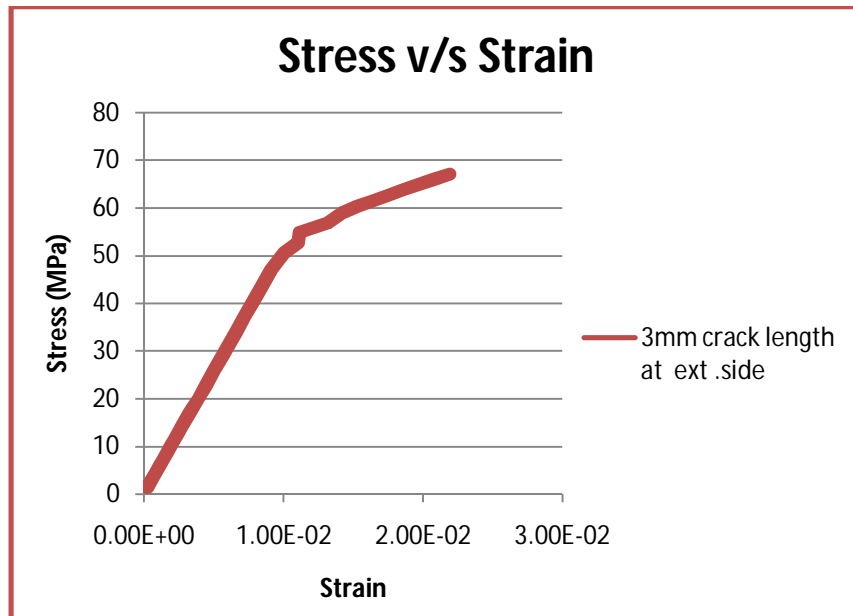


**Figure 15. Stress-strain response when crack is provided outside the overlap joint**

### Conclusions

3D finite element analysis has been performed for the stress analysis of adhesive layer in SLJ made of FRP laminated composites considering laminated adherents possessing orthotropic material property and symmetrically cross ply oriented. Adhesive is considered to be  $0^\circ$  ply orientated, isotropic and nonlinear material property. Twisting moment is applied on top adhered at end of free edge while bottom adhered is fixed. Crack is introduced within and outside the overlap joint for which stress-strain and stress-stress intensity factor responses is studied by varying length of crack and overlapping joint using ANSYS 10.0.

Stress is found to be the maximum at upper corner point of crack tip in adhesive layer in SLJ laminated composites. Stress and stress intensity factor variation is unusual with increase in crack length. Also, increase in lap length of joint results into unpredictable response because of non linear behavior of adhesive material. However, stress intensity factor remains same for all lap lengths. Bond failure between bottom adhered and adhesive layer is found when crack is located within

the overlap joint whereas bond failure between upper adhered and adhesive layer likely to take place when crack is located outside the overlap joint.

### References

- [1] J. P. M. Goncalves et. al., A three dimensional finite element model for stress analysis of adhesive joints, *International Journal of Adhesion and Adhesives*, 22, 357-365, **2002**.
- [2] R.B. Nageswara, R.Y.V.K. Sadasiva, S. Yadagiri, Analysis of composite bonded joints, *Fiber Science and Technology*, 17, 77-90, **1982**.
- [3] Y. Prasanth, G.V.S. Gopinadh, Y. Srinadh et. al., Static analysis of adhesively bonded double lap joint in laminated FRP composites subjected to transverse loading, *International Journal of Engineering Science & Advanced Technology*, 2(2), 263 – 274.
- [4] Y. B. Patil, R. B. Barjibhe, Modal analysis of adhesively bonded joints of different materials, *International Journal of Modern Engineering Research*, 3(2), **2013**.
- [5] B. K. Murthy, R. Venkatakumar, J. Sureshkumar et. al., Fracture analysis of adhesively bonded single lap joint with four layered  $[+\Theta/\Theta]_S$  adherents, *International Journal of Applied Engineering Research*, 1(4), **2011**.
- [6] C. C. Lin, Y. S. Lin, A finite element model of single lap adhesives joints, *International Journal of Solids Structures*, 30(12), 1679-1692, **1993**.
- [7] G. Li, P. Lee-sullivan, R.W. Thring, Non-linear finite element analysis of stress and strain distributions across the adhesive thickness in composite single-lap joints, *Composite Structures*, 46 (4), 395-403, **1999**.
- [8] S.K. Panigrahi, B. Pradhan, Three dimensional failure analysis and damage propagation behavior of adhesively bonded single lap joints in laminated FRP composites, *Journal of Reinforced plastics and Composites*, 26(2), 183-200, **2007**.
- [9] K. Jeong-Ho, H. Glaucio, The interaction integral for fracture of orthotropic functionally graded materials: evaluation of stress intensity factors, *International Journal of Solids and Structures*, 40, 3967–4001, **2003**.

-----

# ANALYSIS OF EARLIEST DEADLINE FIRST AND RATE MONOTONIC SCHEDULING ALGORITHM IN SOFT REAL-TIME SYSTEM

**J. Teraiya\*, Apurva Shah\*\***

\*Computer Engineering Department,  
Marwadi University, Rajkot, India,  
E-mail : jay.teraiya@gmail.com

\*\*Department of Computer Science and Engineering  
The Maharaja Sayajirao University of Baroda, Vadodara, India  
E-mail : [apurva.shah-cse@msubaroda.ac.in](mailto:apurva.shah-cse@msubaroda.ac.in)

## Abstract

The Earliest Deadline First (EDF) is a dynamic scheduling algorithm, and it gives priority to the task based on its absolute deadline; the task having the nearest deadline will have the highest priority. EDF one of the best suitable for scheduling tasks with Soft Real-Time Operating System (RTOS). The Rate Monotonic (RM) algorithm is a static scheduler. It gives priority to the task based on its occurrence period, or we can say it gives priority based on the rate of the task. A task which has the lowest rate will assign the highest priority in the RM algorithm. In this paper has implemented the EDF and RM for the Soft-RTOS. These algorithms have been tested with *the periodic* task set, and observations are gathered. Algorithms are compared based on Success Ratio & Effective CPU Utilization in similar conditions. It has been observed that the EDF algorithm performs well in underload conditions, but in an overload situation, performance gets degraded. Whereas RM not able to schedule specific tasks set in underload condition but it reasonably performs well in an overload condition compare to EDF. Practical experiments have been executed with an extensive process set. Process Set contains a 6000-task set, and every task set has a different number of tasks between one to nine. Every process set also has different CPU utilization factor 0.5 to 5. These algorithms have been evaluated on a 500-time line to validate the performance in all scenarios.

**Keywords:** RTOS, Real-Time Systems, Scheduling, RM, EDF

## 1. Introduction

The usage of Real-Time based systems is getting increased day by day. Developing a system that is expected to generate real-time results need to manage timing constraints of all functionalities. All tasks in RTOS have their related deadlines and have to finish the task within the given deadline. Based on RTOS type, it is necessary to select a scheduler that assigns a task to the processor by taking into considering the timing constraints and supporting all other needs of scheduling. Based on the time criticality, real-time systems divided into three significant categories hard, soft, and firm real-time systems. In Hard RTOS, if the deadline is missed, the disaster will occur even though the miss is minor. A Soft RTOS if the deadline is missed, the disaster will not happen, but the overall performance of the system will degrade [1].

Based on the property of the RTOS and task sequence, the appropriate scheduling method should be applied. In RTOS, the task can be categorized as Periodic, Aperiodic, and Sporadic task. It is also classified based on the non-preemptive or pre-emptive task.

The scheduler is organizing the sequence of tasks such a way that it can satisfy its different conditions. A task has characteristics like execution and arrival time. It also has a deadline, period, and other requirements. The Static and Dynamic algorithms are two types of scheduling algorithm which is used depends on the approach. The scheduler, which assigns priority only once at the time of initialization, is referred to as a Static scheduling algorithm. Rate Monotonic (RM) is one of the examples of static priority scheduler. The scheduler, which keeps changing the priority based on the current situation, is referred to as a dynamic scheduling algorithm. The Earliest Deadline First (EDF) is one of the examples of the dynamic scheduling algorithm. [2][3]. The motivation behind this paper is to evaluate EDF and RM algorithm with different periodic task set. Researchers want to observe the behaviour of these algorithms for different values of Utilization Factor ( $U_p$ ). When value of  $U_p < 1$ , the situation is considered as underload situation and there are many algorithms exist which can schedule given task set. When value of  $U_p > 1$ , the situation is considered as overload situation and there is not a single algorithm exist which can schedule given task set. Researchers have tested these both algorithm in underload and overload situation. This paper has evaluated the Earliest Deadline First and Rate Monotonic schedulers with a diverse scenario. This paper has evaluated these algorithms based on two different

parameters called Effective CPU utilization (ECU) and Success Ratio (SR). Paper has evaluated both schedulers in underload and overload situations [4].

Paper has been arranged in the following way: The scheduling method EDF and RM described in Section 2 and 3. Related work is described in Section 4. Algorithm Evolution Criteria and Practical Setup are described in Section 5. Section 6 discussed the analysis and evaluation of both schedulers, and the paper is ended with a conclusion in Section 7.

## **2. The EDF Algorithm**

The EDF algorithm is a dynamic pre-emptive scheduler. It gives priority to the task based on the absolute deadline. Priorities of tasks are allocated dynamically and are inversely proportional to the absolute deadlines of the active tasks [6][10]. Figure 1 shows the flow of the EDF algorithm. When the currently executing task is completed, or a new task comes, the scheduler will run and check the absolute deadline of each active task. The task which has the earliest deadline will be selected for the next execution. EDF is optimal for scheduling a task set in pre-emptive single processor environment. It means that if a given set of tasks can meet all deadlines, then EDF is able to schedule this task set. If there is an optimal scheduler which meets all deadlines of given task set, and scheduling decisions made by EDF will be identical to those made by optimal scheduler.

## **3. The RM Algorithm**

The RM algorithm is a static pre-emptive scheduler. It gives priority to the task based on its Rate (task occurrence period). The task with the smallest Rate will get high priority [5][6]. The period of any task is pre-defined in RTOS and defined as the task occur again in a given duration. Figure 2 shows the flow of the RM algorithm. When the currently executing task is completed, or a new task comes, the scheduler will run and check the lowest rate of each active task. The task which has the lowest rate will be selected for the next execution [10]. It is known that RM is an optimal fixed priority scheduler for scheduling implicit deadline under pre-emptive single processor environment. If there is any fixed priority scheduler which can schedule a given task set to meet their deadlines of all task, then RM will also able to schedule that task set for all their task.

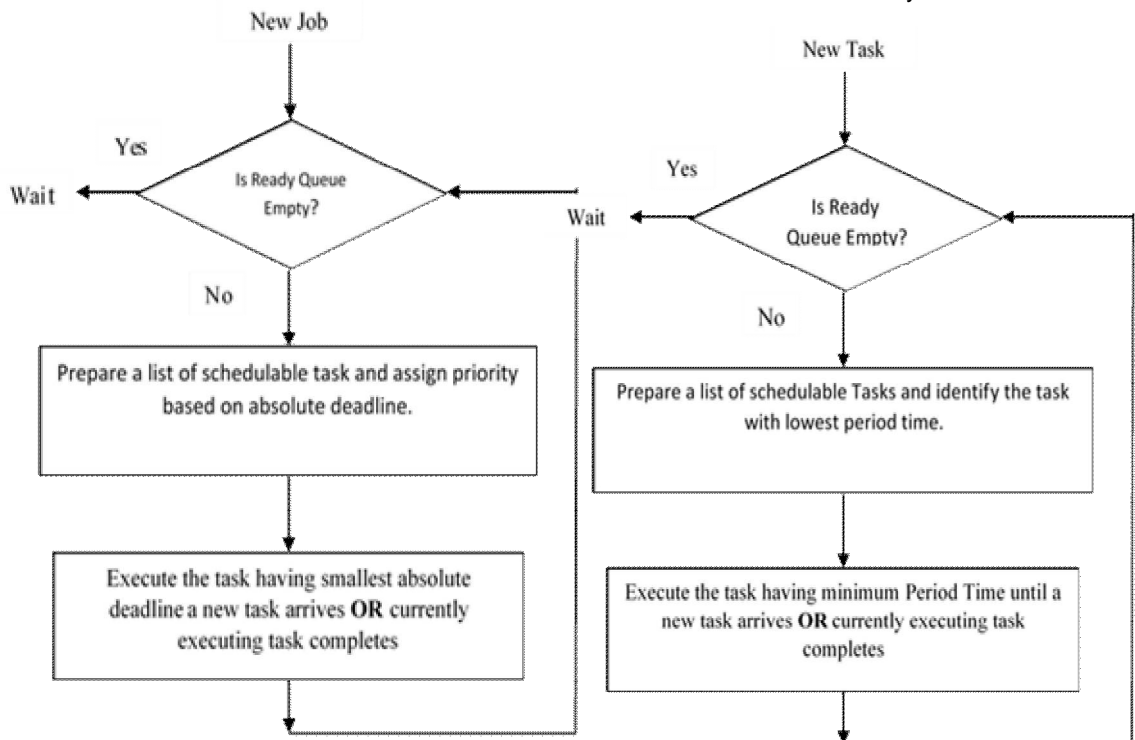


Fig.1 - EDF

Fig.2 - RM

#### 4. EDF and RM Related Work

It is possible to verify the stimulability of any set of the periodic task set. The periodic task set has its deadline ( $D$ ), its occurrence period( $T$ ), and its execution time( $C$ ). The utilization factor  $U = \frac{C}{T}$  gives the time used by the assigned task of the processor. For any point in time, the utilization factor can be calculated with the following equation.

$$U_p = \sum_{i=1}^n \frac{C_i}{T_i} \quad (1)$$

The total CPU utilization factor  $U_p$  states the fraction of processor time used by the periodic task set. The given task set is schedulable or not will be decided based on the value of  $U_p$ . If vale of  $U_p$  is less than 1, then it is possible to schedule the given task set, but if the value of  $U_p$  is greater than one than there is no scheduler exist which can schedule tasks set completely [6].

The EDF assigns priorities based on its absolute deadline. The periodic task can be pre-empted when a new task with the smallest absolute deadline arrives. The EDF scheduler performs well compare to any other static scheduler in underload scenario, and it is possible to schedule all the task within the task set if  $U_p < 1$ [1]. The RM assigns priorities based on its occurrence period (Rate). The scheduler chose the task from the whole ready task with the shortest period to execute next. RM has advantages like easy to implement, it has less runtime overhead, simple to evaluate, and it is predictable in overload scenario [6][7].

### 5. Algorithm Evaluation Criteria and Practical Setup

The Soft-RTOS task set has the required data to calculate the time required to complete the task when the task is dispatched. This paper is assuming that the task set is periodic and pre-emptive. During the evolution of these algorithms, it has been considered that the task does not have any resource clash issue, and it has also been considered that there is no overhead in the pre-emption and scheduling algorithm.

This paper evaluating EDF and RM method, and these algorithms are implemented using the C programming language. These algorithms have been integrated with simulator which has been develop in C language by Researchers. The C language compiler is GNU GCC. The simulator has been executed on hardware configuration – Core i5 processor with 8 GB of RAM. Simulation of the proposed algorithm has been carried out on a 64-bit Windows 10 Enterprise operating system. These algorithms execute and schedule the task as per Figure 1 and Figure 2. This paper has considered a periodic task set for evaluating the performance of the algorithm. The task set has been generated using a software module that is developed in C language. This module has generated a large amount of task set, which has 1 to 9 tasks in each set. Each task set has a different utilization factor, and it varies from 0.5 to 5.0 [11]. At a glance, EDF and RM have been evaluated with more than 30,000+ task to prove its performance. Each task set has been scheduled for a 500-time unit to test the effectiveness of the algorithm.

Evaluation of EDF and RM algorithms have been measured based on following two-parameter

**Success Ratio (SR)** - Soft RTOS expects to meet all the deadlines of a given task in the task set, and it is a crucial parameter for any scheduler to check its performance. This paper is trying to find out that any given task can meet their deadline or not. Because of that essential parameter is SR and it defines as below [8][9],

$$SR = \frac{\text{Number of Task successfully scheduled}}{\text{Total Number of Task arrived}} \quad (2)$$

**Effective CPU Utilization(ECU)** – This parameter will calculate the effective use of CPU. It shows the time which is used by the task to schedule the task and the task which can meet their deadline. ECU defined as:[8][9]

$$ECU = \sum_{t \in R} \frac{V_t}{T} \quad (3)$$

Here,

V represents task value and,

- Value of task = Execution time of the task, if it completes its execution before its deadline.
- Value of task = 0, if the task miss deadline.
- R is a set of tasks, which are scheduled successfully, i.e., completed within their deadline.
- T is the total time of scheduling.

## 6. Result and Discussion

EDF and RM algorithm has been evaluated on the simulator, which is developed in the C programming language. Results have been gathered and represented in Table I and Table II. Underload scenario results have been displayed in Table I, where task set have utilization factor which is less than or equal to 1. It has been observed that EDF can meet all the deadlines, whereas RM is missing a few of them. Based on this observation, we can say that the EDF algorithm is advisable in the underload scenario compare to RM. Overload scenario results have been displayed in Table II, where task set have utilization factor which is greater than 1. Table II reflects a significant performance difference between EDF and RM in the overload scenario. If the utilization factor is more than 1 for any given task set than it is not possible to schedule a task set, and few of their task will miss their deadline. Table II observation says that EDF performance degraded very rapidly in slightly overload situations, whereas RM is still able to meet a few of their deadlines. Table I and Table II have been represented in the plotted graph in Figure 3 and Figure 4.

**Table 1. Underload Scenario**

<b>Load</b>	<b>ECU%</b>		<b>SR%</b>	
	<i>EDF</i>	<i>RM</i>	<i>EDF</i>	<i>RM</i>
0.50	49.49	49.49	100.00	100.00
0.55	54.66	54.40	100.00	100.00
0.60	59.39	59.39	100.00	100.00
0.65	64.35	64.35	100.00	100.00
0.70	69.35	69.35	100.00	100.00
0.75	74.31	74.31	100.00	100.00
0.80	79.22	79.22	100.00	100.00
0.85	84.16	84.16	100.00	100.00
0.90	89.16	89.15	100.00	99.99
0.95	94.17	94.08	100.00	99.93
1.00	99.10	97.78	100.00	98.92

**Table 2. Overload Scenario**

Load	ECU%		SR%	
	<i>EDF</i>	<i>RM</i>	<i>EDF</i>	<i>RM</i>
1.05	17.45	70.85	18.27	78.49
1.10	9.21	75.82	9.31	80.49
1.15	6.29	73.20	6.19	75.88
1.20	4.62	83.50	4.22	79.47
1.25	4.06	79.05	3.67	77.58
1.30	3.63	75.66	3.19	73.81
1.35	3.12	74.65	2.65	70.77
1.40	2.66	83.55	2.24	75.47
1.45	2.50	79.75	2.00	69.03
1.50	2.21	85.27	1.71	70.33
1.60	2.17	85.61	1.61	69.52
1.70	2.03	86.26	1.42	65.99
1.80	1.93	86.12	1.30	65.98
1.90	1.90	85.83	1.29	63.51
2.00	1.84	85.78	1.20	62.88
2.25	1.76	84.27	1.04	56.16
2.50	1.55	87.06	0.89	53.82
2.75	1.46	89.21	0.78	52.07
3.00	1.32	94.46	0.63	48.36
3.50	1.27	93.48	0.57	44.50
4.00	1.11	95.04	0.43	39.52
4.50	1.08	96.77	0.38	36.45
5.00	0.97	98.13	0.31	31.72

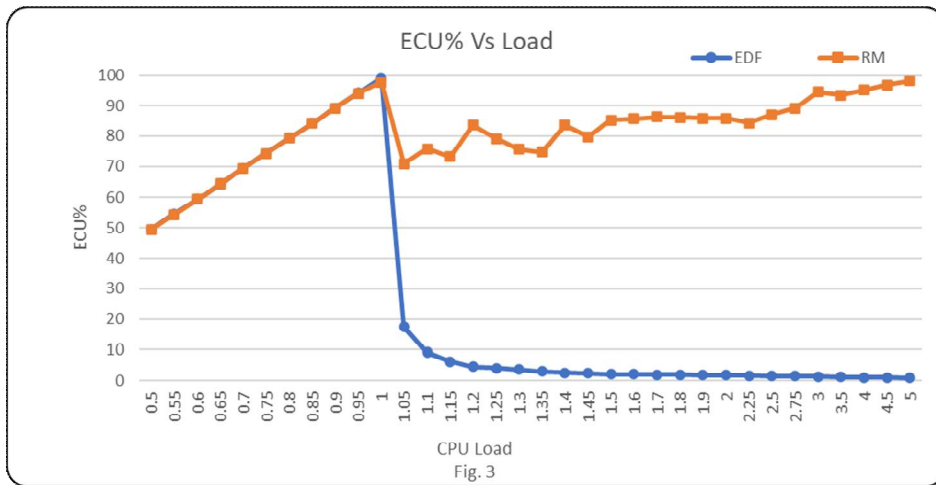


Fig. 3

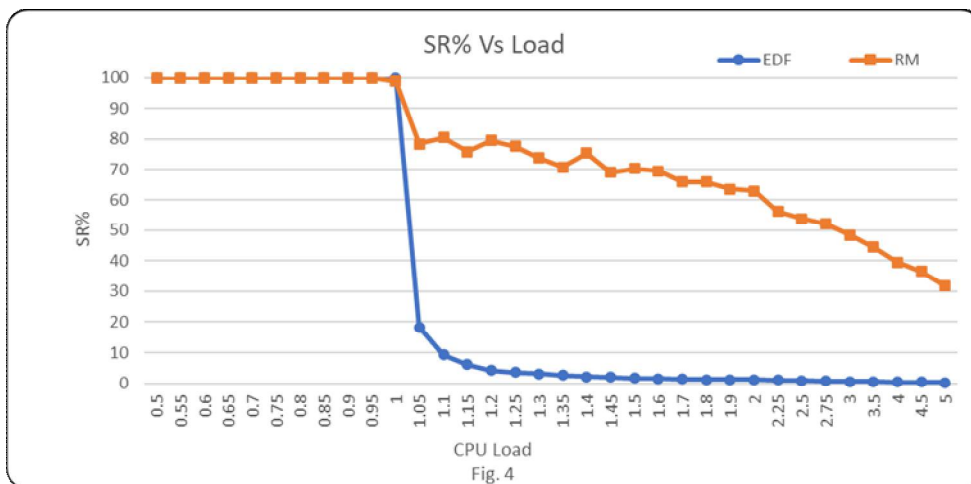


Fig. 4

**Conclusions**

This paper has assessed the EDF and RM scheduling methods for Soft RTOS by considering the periodic task set with a single processor and also believed that the task set is pre-emptive. A comparison of results is given in Table I, which suggests that the EDF, which is dynamic scheduling methods, meets a 100% deadline in the given task set in the underload scenario. In contrast, it is possible to schedule a given task set, but RM failed to schedule it.

In an overload scenario, which results described in Table II, where the EDF scheduling method misses most of the deadline in the given task set, whereas the

RM scheduling method still able to meet some the deadline and performs well compared to EDF. Based on the above practical observation, it is advisable to use EDF (dynamic scheduling method) in the underload scenario, whereas RM (static scheduling method) in overload scenario so scheduling method will get more effectiveness.

## References

- [1] R. Belagali, S. Kulkarni, V. Hegde, and G. Mishra, "Implementation and validation of dynamic scheduler based on LST on FreeRTOS," 2016 Int. Conf. Electr. Electron. Commun. Comput. Optim. Tech. ICEECCOT 2016, pp. 325–330, 2017.
- [2] F. Lindh, T. Otnes, and J. Wennerström, "Scheduling algorithms for real-time systems", Dep. Comput. Eng. Malardalens Univ. Sweden, 2010.
- [3] D. Thakor and A. Shah, "D\_EDF: An efficient scheduling algorithm for real-time multiprocessor system," Inf. Commun. Technol. (WICT), 2011 World Congr., pp. 1044–1049, 2011.
- [4] J. Teraiya and A. Shah, "Comparative Study of LST and SJF Scheduling Algorithm in Soft Real-Time System with its Implementation and Analysis," 2018 Int. Conf. Adv. Comput. Commun. Informatics, ICACCI 2018, pp. 706–711, 2018.
- [5] W. Li, K. Kavi, and R. Akl, "A non-preemptive scheduling algorithm for soft real-time systems," Comput. Electr. Eng., vol. 33, No. 1, pp. 12–29, 2007.
- [6] G. C. Buttazzo, "Rate Monotonic vs. EDF: Judgment day," Real-Time Syst., Vol. 29, No. 1, pp. 5–26, 2005.
- [7] G. Chen and W. Xie, "On a laxity-based real-time scheduling policy for fixed-priority tasks and its non-utilization bound," 2011 Int. Conf. Inf. Sci. Technol. ICIST 2011, pp. 7–10, 2011.
- [8] K. Ramamritham, J.A.Stankovik, and P.F.Shiah, "Efficient scheduling algorithms for real-time multiprocessor systems," IEEE Transaction on Parallel and Distributed Systems, Vol. 1, April 1990.
- [9] Shah, A., & Kotecha, K. Scheduling Algorithm for Real-Time Operating Systems Using ACO. In Computational Intelligence and Communication Networks (CICN), 2010 International Conference on (pp. 617-621). IEEE. November 2010.
- [10] Mohammadi, A., & Akl, S. G. Technical Report No. 2005-499 Scheduling Algorithms for Real-Time Systems\*. 2005.
- [11] <http://processdataset.in/>

-----

# FINET: FACIAL EXPRESSION RECOGNITION BASED ON FUSION INHERITED NETWORK

V. Mokaya<sup>1</sup>, M. Gupta<sup>2</sup>, M. Bansal<sup>3</sup>

<sup>1</sup>Department of Computer Science & Information Technology,  
Suresh Gyan Vihar University, India  
E-mail : victor.mokaya@mygyanvihar.com

<sup>2</sup>Department of Electrical Engineering, Suresh Gyan Vihar University, Jaipur, India  
E-mail : [mukeshkr.gupta@mygyanvihar.com](mailto:mukeshkr.gupta@mygyanvihar.com)

<sup>3</sup>Department of Software Engineering, Altran Private Limited, India  
E-mail : [mukesh.bansal@altran.com](mailto:mukesh.bansal@altran.com)

## Abstract

Machine learning models built from complex hand-crafted features and classification processes are challenging to design and aren't robustized. Due to this fact, convolutional architecture is incorporated to automatically extract and classify class labels with high levels of accuracy. In this work we propose a lightweight network FiNet: fusion inherited network for universal facial expression recognition. FiNet consists of two fusion blocks for contextual feature extraction from salient regions. Block-1 uses a single convolution filter to capture and preserve the domain features. Block-2 dispenses unwanted features from the enriched inherited features by employing a single filter. The inherited results of block one and two are fused into block 3 which merge all the comprehensive region features for classification by discriminating for higher adaptability. The two-stage fusion network significantly allows the network to only conserve spatial features which increases the discriminative power of FiNet. Space computation complexity is achieved by limiting the number of parameters and incorporating smaller database size which proves the reliability of FiNet. FiNet size is 3.6MB as compared to VGG16:500.5MB, and ResNet 88.4MB. Comparative analysis on ResNet and VGG16 proved that the results of our proposed model outperformed existing futuristic models. The recognition accuracy results of our model on JAFFE and CK+ database was 84.37% and 96.62% respectively. The proposed model provides higher adaptability to lower computational power and storage as compared to traditional systems. FiNet size is 3.6MB compared to VGG16:500.5MB, and ResNet 88.4MB. FiNet provides an opportunity to be deployed in smart gadgets.

**Keywords:** Facial Expression Recognition, fusion, space computation complexity, Feature Classification, FiNet

## 1. Introduction

Expressions convey the most effective information about the mental process and intentions of the speaker during communication [1]. Nowadays with advancement of human computer interaction (HCI) it is necessary to monitor all the practical and essential activities about education, entertainment, psychiatric treatment, reviewing online shopping experience, and monitoring driver fatigue for long distance travels. At present HCI systems provide better and reliable performance results but their robustness still needs improvements to enhance efficiency. Currently the principal feature expression recognition (FER) approaches are: Action Units (AUs) [2] and appearance-based methods. Decoding facial landmarks reveals a composition of AUs; 12 on the upper and 18 on the lower face. They record the expansion or contraction of the facial muscles (eye, nose, mouth, burrows, lips, eyebrows, and eye corners). The appearance of the primary details however remains intact during this task. Appearance based methods largely rely on large image samples to detect multiple characteristics (face shape, eye color, mouth closed, mouth opened and skin color). Another class of approaches which incorporates hand crafted feature descriptors include Principal Component Analysis (PCA) [3], Discrete Cosine Transform (DCT) [4], Gabor features [5], Haar-like features [6] and Local Binary Pattern (LBP) [7]. After extraction, the above features are fed into a feature classifier in form of feature map or feature vector for classification. Nowadays with providence of computing power and cutting-edge technology, convolution neural network (CNN) have become the sort after techniques for computer vision tasks. Major applications include; object detection, face recognition, facial expression detection, haze removal, and anomaly detection among others. Implementation of CNN includes adjusting and updating the weights of the inputs in order to learn the sufficient class labels. Latest proposed models in literature include; a model similar to VGG16 by [8] was achieved through fine tuning the network parameters. A Weighted Mixture Deep Neural Network (WMDNN) [9] with two color channels for gray-scale and color images were proposed According to [10] an ensemble model for transfer learning using VGG16 and SVM classifier is proposed. In work done by [11], a novel Deep Attentive Multi-path CNN (DAM-CNN) is proposed which yields a dynamic image representation for FER. According to [12] a three VGG-net and Long Short-Term Memory (LSTM) [13] is proposed. The VGG-net extracts static and motive features whereby three types of attention mechanisms are jointly integrated for discriminative visual representation. The descriptive micro-expression features are fed into LSTM to extract spatial features

FiNet: facial expression recognition ..... inherited network

for micro-expressions recognition. According to work by [14] a region-based pattern with an extensive index for response to emotions known as (RETRaIN) is developed.

## 2. Proposed method

FiNet has been implemented by reducing the block size of the convolution layers and increasing the filter size. The blocks consist of down-sampling max pooling with filter size 2x2 to extract macro features comprehensively. VGG16-Net has been developed on deep dense networks suitable for computer vision applications. However, deep dense has been unlikely to capture macro level features of expression locations due to larger convolution and pooling tasks. Therefore, to reduce space computation complexity a shallow lightweight network is proposed to extract adequate spatial information from facial expressions. Additionally, an embedded discriminative layer to enhance class category capabilities is incorporated.

Our proposed FiNet architecture has three blocks. The proposed architecture is as follows: the initial block has one 5x5 convolution layer and 6 filters over the input image to retrieve fine features (brows, burrows, eye lines etc.); the intermediate block of one 5x5 convolution layer and 16 filters extracts course feature (eyes, mouth, lips, chin, nose etc.). The resultant inherited features from layer one and two are fused together and fed to the final block with one 5x5 convolution layer and 32 filters to employ discriminative extraction of active feature regions. In each block except the last there exists a max pooling layer with filter size 2x2 to capture feature maps of highest pooling value. The two output layers consist of 84 neurons and a classification layer with 7 neurons to represent the 7 expression classes. The proposed model is shown in Table 1 below. Figure 1. shows the flowchart of experimental procedure.

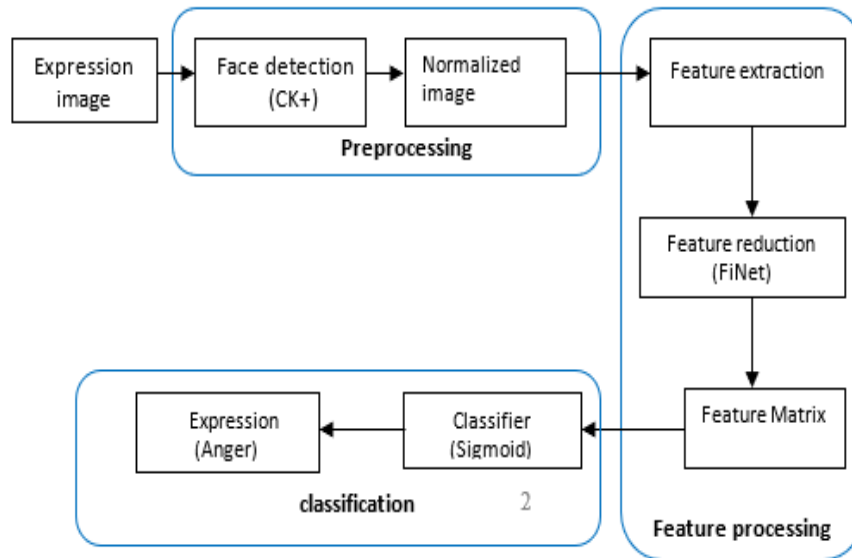


**Figure 1. Flow chart of experimental procedure**

**Table 1. The proposed FiNet network**

Input image: 128 x128x1
Conv2d: 5x5x6 + ReLu
Maxpooling: 2x2
Conv2d:5x5x16 +ReLu
Maxpooling:2x2
Conv2d:5x5x32 +ReLu
FC:84 + ReLu
FC: 7

## 2.1. Pre-processing

In the pre-processing we normalized the images for saliency and to retain spatial features. Original image size 256 x 256 was cropped and scaled to 128 x 128 by elimination of ground influences. Further on we detected the eyes which were the salient regions from the cropped image. The face was further rotated by the angle between y-axis and x-axis, this was necessary in order to preserve the salient regions as shown in figure.2 below.

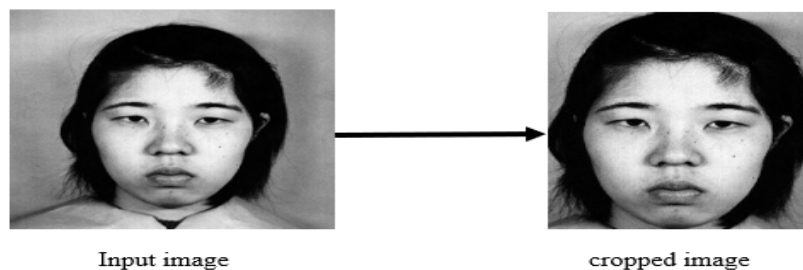


**Figure 2. Pre-processed JAFFE dataset**

## 2.2. Feature training

For training we minimized the cost function using batch gradient descent and modified the weights using the back-propagation error algorithm [15]. Batch size was set to 255 and the momentum of the weights 0.15. Drop out was utilized to prevent overfitting to the fully connected layers (except for the last output layer) with probability of 0.25. Experimental results prove the learning rate increased to the tens digit after every 5 epochs and remained constant at the 90<sup>th</sup> epoch. The network was trained with 100 epochs. In the experiment the bias was initialized by zero and all weights randomly initialized with normal distribution of mean zero and standard deviation set to as in equation Eq. (1) below.

$$\delta = \sqrt{\frac{2}{x}} \quad (1)$$

Where  $x$  = weight size on each neuron, c.l (Convolution Layer) and f.c.l (Fully Connected Layer). c.l of  $x$  = (filter size) x (filter size) x (depth of previous layer), f.c.l of  $x$  = number of neurons from previous layer in each iteration, 255 images

were injected into the network. After each iteration the training data was shuffled randomly. Cross-entropy was applied in the following pattern in equation Eq. (2)

- $M$  represents the size of images in the training set
- $E$  represents the size of emotion labels
- $y_n$  is the one-hot encoding of the true class label of  $n^{\text{th}}$  image.
- $\hat{y}$  probability distribution of emotion classes of  $n^{\text{th}}$  image using SoftMax function.

Cross- entropy equation is given by:

$$Z = \frac{1}{M} \sum_{n=1}^M \sum_{p=1}^E y_n(p) \log(\hat{y}_n(p)) \quad (2)$$

Where  $y_n(p) \in (0,1)$  and  $p$  is the true label of  $n^{\text{th}}$  image.  $\hat{y}_n(p) \in (0,1)$  represents probability is the true label of  $n^{\text{th}}$  image.

### 2.3. Feature testing

The dataset was grouped into two sets. During training highest accuracy levels were injected into the test set for validation. Further, the final validation set accuracy presented the recognition intelligence of our system for the emotion classes. The results of the predicted labels are shown in figure 2 and figure 3 below.

Further, we regularized the weights of each layer to limit size of the individual layer by adding a value to the hyperparameter. The given neuron result is represented by rectified linear unit  $y$  and the dropout possibility probability given by  $y, d$  in equations Eq. (3) and Eq. (4) below.

$$f(y) = \max(0, y) \quad (2)$$

$$Dropout(y, d) = \sum_{y, prob, 1-d}^{y, prob, d} y \quad (3)$$

### 3. Results and discussion

Our model results were analyzed with futuristic architecture built on similar database. The different techniques used for analysis of results were; LBP [7], LDP [16], and LDN [17], ResNet [18], and VGG16[8]. Current CNN models like VGG16 -Net and ResNet have recorded impressive classification results. However, in FER tasks these models fail to conserve discriminative features. Recent studies [19] confirm that deep neural networks fail to learn sufficient features over smaller datasets. Moreover, present FER benchmark datasets have limited sample sizes. Therefore, to overcome this challenge we developed a shallow and lightweight model to extract sufficient features with smaller parameters. FiNet network has eight million (8M) parameters while VGG-16:138M and ResNet 31M. Thus, FiNet has a higher adaptability to handle real world challenging tasks together with lower computational power as compared to the latter. FiNet weighs 3.6MB compared to VGG16:500.5MB, and ResNet 88.4MB. This provides FiNet a niche higher to be deployed in smart gadgets. The performance and accuracy of the proposed work on CK+ dataset was recorded in Table 3. The comparison of our model was evaluated with high accuracy benchmark model over the same database LBP [7], Local Directional Pattern (LDP) [16] and Local Directional Number (LDN) [17]. Our model performed better with high accuracy of 96.62% against the other methods that were compared for 7 classes. The evaluation of our results was further performed on JAFFE and CK+. Figure 3. and Figure 5 below illustrates the train loss versus validation loss for JAFFE and CK+ dataset. Figure. 4. and Figure. 6. below illustrates the training accuracy and validation accuracy for both JAFFE and CK+ database for 7 motions. The performance accuracy of our results was evaluated with other benchmarks. Our model attained 84.38% accuracy against other models as illustrated above in Table 3.

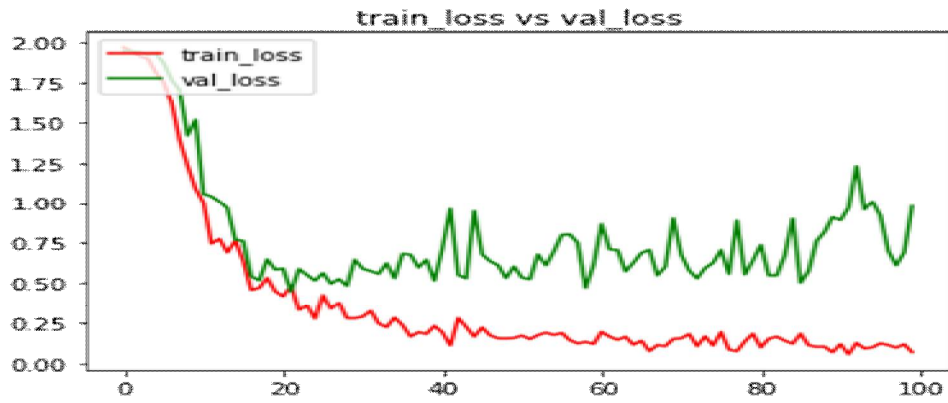


Figure 3. Training loss vs validation loss for JAFFE dataset

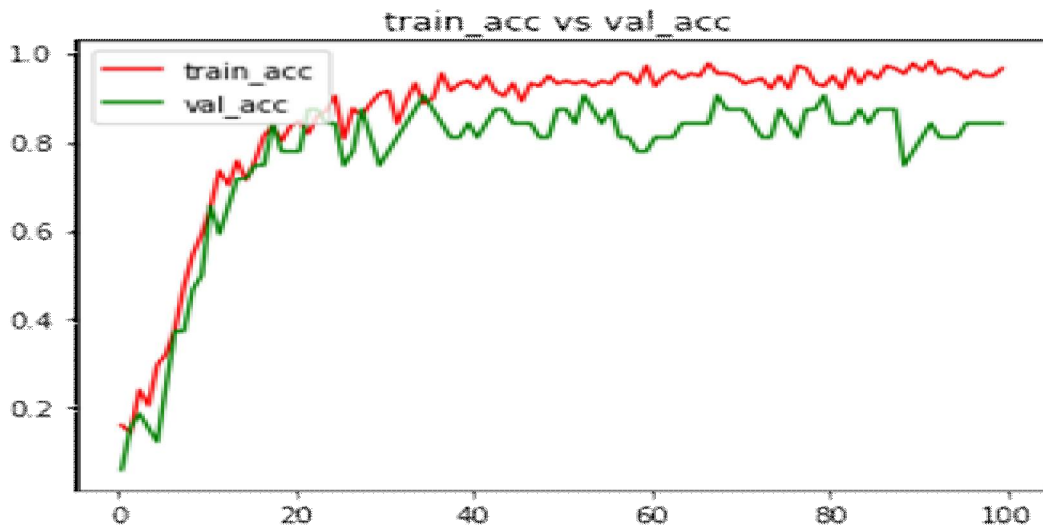
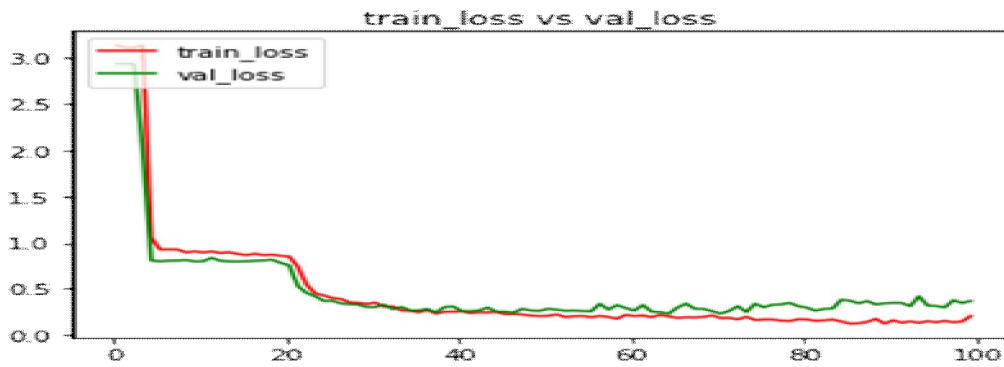
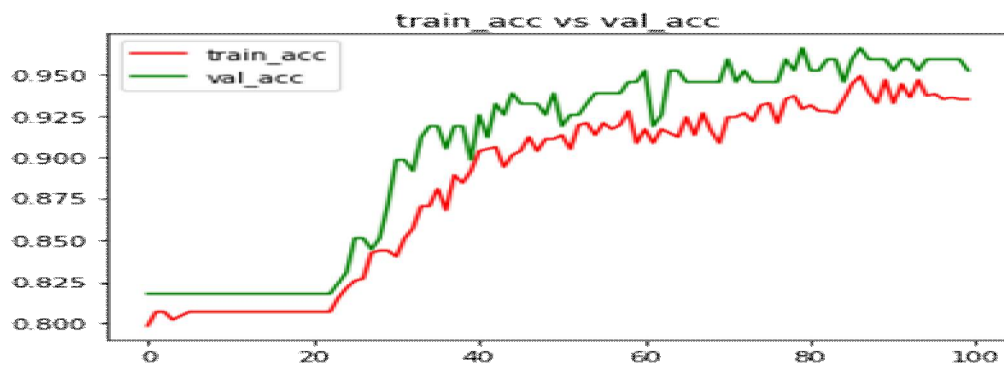


Figure 4. Training accuracy vs Validation accuracy for JAFFE dataset



**Figure 5. Training loss vs validation loss for CK+ dataset**



**Figure 6. Training accuracy vs Validation accuracy for CK+ dataset**

Table 2, Facial Expression Rate (%) of our model and other methods on JAFFE and CK+ for 7 classes.

Method	7 class labels	7 class labels
	JAFFE	CK+
	Accuracy %	Accuracy %
LBP [7]	85.23	89
LDP [16]	86.19	92.3
VGG16[8]	85.1	95.2
ResNet[18]	85.6	91.8
LDN [17]	81.42	91.68
<b>FiNet</b>	<b>85.38</b>	<b>96.62</b>

### 3.1. Extended Cohn Kanadedatabase

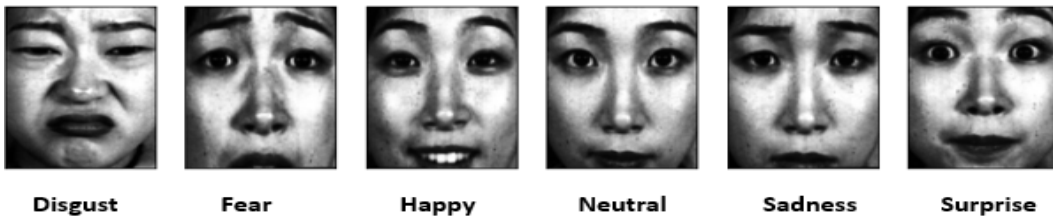
The CK+ database consists of 1043 facial expression images from 123 subjects of different age groups [20]. Figure 7. shows samples from CK+ dataset. From these, 981 images were used with seven expression states: Anger, Happy, Sad, Neutral, Fear, Contempt and Surprise. The images were divided as follows: 80% training sample and 20% testing sample



Figure 7. Sample of CK+ Dataset

### 3.2. JAFFE database

Our performance metrics were conducted using the JAFFE [21]. Inside the database were 213 peak emotions of the ten subjects in the dataset. In this dataset each subject comprises of six universal emotions (Anger, Happy, Sad, Contempt, Neutral, Fear and Surprise). Figure 8. Shows sample images from JAFFE dataset.



In our model 198 images were used, 80:20 ratio was used for training and testing phases.

Figure 8. Sample of JAFFE Dataset

## Conclusions

In this work a novel CNN architecture FiNet: fusion inherited network is proposed for macro facial expression recognition. We have proposed two blocks and single block of convolution layers fused together with filter size 5x5, to retrieve comprehensive and enriched features from salient regions. The weights of convolution filters are however 6,16 and 32 respectively for each block. FiNet utilizes the third block for enhanced discrimination of preservation of enriched features. The effectiveness of FiNet was examined on similar CNN variants for performance. The experimental setup was tested on two benchmark datasets Ck+ and JAFFE with profound classification accuracy results. We plan to enhance our work by using different transfer architecture to detect features from this network and SVM to categorize emotion classes from micro-features of facial expressions.

## Acknowledgement

I wish to thank my supervisor Dr (prof) Mukesh Kr. Gupta for the immense support and guidance during the preparation of this work. The continued support and assistance from Dr Mukesh Bansal were also helpful to complete this work successfully.

## References

- [1] Ekman, Paul., "*Facial expression and emotion*". American psychologist, 1993.
- [2] Emily Prince, Martin Katherine, Messinger Daniel, Allen Mike, "Facial action coding system". *The SAGE Encyclopedia of Communication Research Methods*, 2017.
- [3] Lever, Jake, Martin Krzywinski, and Naomi Altman, Points of significance: "*Principal component analysis*", Nature Publishing Group. 2017,
- [4] Hayat, Khizar, and Tanzeela Qazi. "Forgery detection in digital images via discrete wavelet and discrete cosine transforms." *Computers & Electrical Engineering* Vol.62,pp 448-458, 2017.
- [5] Wu, T., Bartlett, M. S., & Movellan, J. R. "*Facial expression recognition using gabor motion energy filters*". IEEE computer society conference on computer vision and pattern recognition-workshops", pp. 42-47, 2010.

- [6] Mohamed, B., Issam, A., Mohamed, A., & Abdellatif, B. "ECG image classification in real time based on the haar-like features and artificial neural networks", *Procedia Computer Science*, Vol.73, pp.32-39, 2015.
- [7] Lin, J. H., Lazarow, J., Yang, A., Hong, D., Gupta, R., & Tu, Z., "Local binary pattern networks", *The IEEE Winter Conference on Applications of Computer Vision* pp. 825-834, 2020.
- [8] Simonyan, Karen, and Andrew Zisserman. "Very deep convolutional networks for large-scale image recognition." *arXiv preprint arXiv*, 2014.
- [9] Yang, B., Cao, J., Ni, R., & Zhang, Y, "Facial expression recognition using weighted mixture deep neural network based on double-channel facial images". *IEEE Access*, Vol.6, pp.4630-4640. 2017.
- [10] Nyein, T., &Oo, A. N. "University Classroom Attendance System Using FaceNet and Support Vector Machine". *International Conference on Advanced Information Technologies (ICAIT)*, pp. 171-176, IEEE. 2019.
- [11] Cha, Young. Jin, Wooram Choi, and Oral Büyükoztürk, "Deep learning-based crack damage detection using convolutional neural networks. *Computer-Aided Civil and Infrastructure Engineering*". 2019.
- [12] Yang, T., Wu, Y., Zhao, J., & Guan, L. "Semantic segmentation via highly fused convolutional network with multiple soft cost functions", *Cognitive Systems Research*, Vol.53, 2019.
- [13] Greff, K., Srivastava, R. K., Koutník, J., Steunebrink, B. R., &Schmidhuber, J. LSTM: "A search space odyssey". *IEEE transactions on neural networks and learning systems*, Vol.28, 2016.
- [14] Verma, M., Vipparthi, S. K., & Singh, G "Region Based Extensive Response Index Pattern for Facial Expression Recognition". *International Conference on Communication, Computing and Internet of Things (IC3IoT)*, pp. 20-24,2018.
- [15] Cilimkovic, Mirza. "Neural networks and back propagation algorithm." *Institute of Technology Blanchardstown, Blanchardstown Road North Dublin* 2015.
- [16] Rivera, A. R., Castillo, J. R., & Chae, O. O. "Local directional number pattern for face analysis: Face and expression recognition". *IEEE transactions on image processing*, 22(5), pp.1740-1752. 2012.
- [17] Pillai, A., Soundrapandiyam, R., Satapathy, S., Satapathy, S. C., Jung, K. H., & Krishnan, R. "Local diagonal extrema number pattern: A new feature descriptor for face recognition", *Future Generation Computer Systems*, Vol. 81, pp.297-306,2018.
- [18] He, K., Zhang, X., Ren, S., & Sun, J. "Deep residual learning for image recognition". *Proceedings of the IEEE conference on computer vision and pattern recognition* pp. 770-778, 2016.

- [19] Schindler Alexander, Thomas Lidy, and Andreas Rauber. “*Comparing Shallow versus Deep Neural Network Architectures for Automatic Music Genre Classification. in FMT*”. 2016
- [20] Lucey, P., Cohn, J. F., Kanade, T., Saragih, J., Ambadar, Z., & Matthews, I. “*The extended cohn-kanade dataset (ck+): A complete dataset for action unit and emotion-specified expression*”. IEEE computer society conference on computer vision and pattern recognition-workshops pp. 94-101. 2010.
- [21] Lyons, M., Akamatsu, S., Kamachi, M., & Gyoba, J. “*Coding facial expressions with gabor wavelets*”. In Proceedings Third IEEE international conference on automatic face and gesture recognition, pp. 200-205.1998.

-----

**Statement about the ownership and other particulars about newspapers  
JOURNAL OF THE MAHARAJA SAYAJIRAO UNIVERSITY OF BARODA**

(To be published in the first issue every year after the last day of February)

**FORM IV**

**(See Rule 8)**

1. Place of the Publication : The Maharaja Sayajirao University of Baroda  
The Maharaja Sayajirao University of Baroda,  
Vadodara - 390 002.
2. Periodicity of its Publication : Science & Technology  
two times in a year.
3. Printer's Name : Shri Jatin H. Somani  
Nationality : Indian  
Address : Manager, The Maharaja Sayajirao University  
of Baroda Press (Sadhana Press),  
Vadodara - 390 001.
4. Publisher's Name : Prof. C. N. Murthy  
Nationality : Indian  
Address : The Maharaja Sayajirao University of Baroda  
Vadodara - 390 002.
5. Editor's Name : Prof. C. N. Murthy  
Nationality : Indian  
Address : The Maharaja Sayajirao University of Baroda  
Vadodara - 390 002.
6. Names & Addresses of Individuals : The Maharaja Sayajirao University of Baroda  
who own the newspaper and  
partners or shareholders holding  
more than one percent of the  
total capital  
Vadodara - 390 002.

I, C. N. Murthy declare that the particulars given above are true to the best of my knowledge and belief.

**Prof. C. N. Murthy**

## **JOURNAL OF THE MAHARAJA SAYAJIRAO UNIVERSITY OF BARODA**

The Journal is mainly intended to publish original research papers contributed by the teachers and research scholars of The Maharaja Sayajirao University of Baroda after undergoing a peer review process. All submitted articles are subject to *anti plagiarism* check before being sent for review. Proceedings of Conferences held within The Maharaja Sayajirao University of Baroda are also accepted for publication subject to the individual articles being peer reviewed.

The Journal is issued every year in three parts. These parts are devoted respectively to topics relating to 1. Science & Technology, 2. Humanities and 3. Social Science. All manuscripts for review to the Science & Technology part should be addressed to:

The Editor (Science & Technology),  
Journal of The M.S. University of Baroda,  
A.I.C.S. Training Centre,  
Vadodara - 390 002.

email: [editor.msujst@gmail.com](mailto:editor.msujst@gmail.com)

Contributors are requested to submit manuscripts, by email attachment which should be typed with double spacing. Authors are advised to retain a copy of the paper that they send for publication as the Editors cannot accept responsibility for any loss of manuscripts not accepted for publication in the Journal.

Authors of papers printed in the Journal are entitled to one copy of the issue free of charge.

### **ADVERTISEMENT**

All advertising matters should be send so as to reach the office of the Journal a month before the publication of the Journal. Further information on rates and space can be had on writing to **[editor.msujst@gmail.com](mailto:editor.msujst@gmail.com)**.



"The full-blown lotus growing out of the lake symbolises the emergence of the mind and its triumph over matter. The flame rising from the center of the lotus is the flame of the human knowledge, spreading light and learning for the coming generations. The motto inscribed below the lotus defines the purpose and existence of life which is love of beauty, goodness and intellectual curiosity."

### महाराजा सयाजीराव विश्वविद्यालय गीत

अमे वडोदराना विद्यापीठनां सपनां सारवनारा  
अमे ज्योत जलावी सृष्टि नवली सहसा सर्जनहारा.

अमे गगनकुसुम कर धरनारा  
अमे मगन मगन थई फरनारा  
अगनबाथ अमे भरनारा  
अमे दैन्यतिमिरने हरनारा.

श्री सयाजी विद्यापीठना ज्ञानदीपने धरनारा  
सत्यं शिवं सुन्दरम् नो मंत्र अनंतर भणनारा.

*श्री सयाजीराव*